

Baryon acoustic oscillation, Hubble parameter, and angular size measurement constraints on the Hubble constant, dark energy dynamics, and spatial curvature

Joseph Ryan,¹[★] Yun Chen,²[†] and Bharat Ratra,¹[‡]

¹*Department of Physics, Kansas State University, 116 Cardwell Hall, Manhattan, KS 66502, USA*

²*Key Laboratory for Computational Astrophysics, National Astronomical Observatories, Chinese Academy of Sciences, Beijing, 100012, China*

Accepted XXX. Received YYY; in original form ZZZ

ABSTRACT

In this paper we use all available baryon acoustic oscillation and Hubble parameter data to constrain six dark energy cosmological models, both spatially flat and non-flat. These data mildly favor (at 1.3-1.4 σ) closed spatial hypersurfaces in the dynamical dark energy models, and favor dark energy dynamics (at > 1-2 σ , depending on the model) over a cosmological constant Λ . They also favor, at 2.2 σ to 3.5 σ , depending on the model, a lower Hubble constant than what is measured from the local expansion rate by Riess et al. (2018).

Key words: (*cosmology:*) cosmological parameters – (*cosmology:*) observations – (*cosmology:*) dark energy

1 INTRODUCTION

The universe is currently undergoing accelerated cosmological expansion. The simplest cosmological model compatible with this acceleration is the standard Λ CDM model (Peebles 1984), in which the acceleration is powered by a spatially-homogeneous energy density that is constant in time (a cosmological constant Λ). The standard Λ CDM model is consistent with many observational constraints (Alam et al. 2017; Farooq et al. 2017; Scolnic et al. 2018; Planck Collaboration 2018) if Λ contributes about 70% of the current energy density budget with cold dark matter (CDM) being the next largest contributor, at a little more than 25%.

The standard Λ CDM model assumes flat spatial hypersurfaces. It has been argued that cosmic microwave background (CMB) anisotropy measurements show that spatial hypersurfaces are very close to being flat, but the recent Planck Collaboration (2016) and Planck Collaboration (2018) CMB anisotropy data analyses in the non-flat case are based on a somewhat arbitrary primordial power spectrum for spatial inhomogeneities. A physically consistent primordial inhomogeneity energy density power spectrum can be generated by inflation, and non-flat inflation models exist which can be used to compute such a power spectrum (for the models, see Gott 1982, Hawking 1984, and Ratra 1985;

for the power spectra, see Ratra & Peebles 1995 and Ratra 2017).¹

When these power spectra (Ratra & Peebles 1995; Ratra 2017) are used in a non-flat Λ CDM model analysis of Planck Collaboration (2016) CMB anisotropy data and a large compilation of non-CMB data (Ooba et al. 2018b; Park & Ratra 2018a), a mildly closed Λ CDM model with $\sim 1\%$ spatial curvature contribution to the current cosmological energy budget is favored at over 5 σ . A similar spatial curvature contribution is favored in dynamical dark energy XCDM and ϕ CDM models (in which dark energy is modelled as an X-fluid and scalar field, respectively; see Ooba et al. 2018c,d, Park & Ratra 2018b,d). These closed models provide better fits to the low multipole CMB anisotropy data, but the flat models are in better agreement with the higher multipole CMB anisotropy data. The non-flat models are in better agreement with weak lensing measurements, but do a worse job fitting higher redshift cosmic reionization data (Mitra et al. 2018, 2019) and deuterium abundance measurements (Penton et al. 2018).²

¹ These non-flat inflation models are slow-roll models, so quantum mechanical fluctuations during inflation in these models result in an untilted primordial power spectrum. It is possible that these power spectra are too simple, but they are physically consistent; it is not known if the power spectrum used in the Planck non-flat CMB analyses are physically consistent.

² Overall the standard tilted flat Λ CDM model has a lower total χ^2 than the non-flat models, lower by $\Delta\chi^2 \sim 10$ -20, depending on

[★] E-mail: jwryan@phys.ksu.edu

[†] E-mail: chenyun@bao.ac.cn

[‡] E-mail: ratra@phys.ksu.edu

It has also been found that spatially-flat dynamical dark energy Λ CDM and ϕ CDM models provide slightly better overall fits (lower total χ^2) to the current data than does flat Λ CDM (in the best-fit versions of these models the dark energy density has only very mild time dependence; see [Ooba et al. 2018a](#), [Park & Ratra 2018b,d](#), and [Sola et al. 2018](#)).³

The constraints on spatial curvature and dark energy dynamics discussed above make use of CMB anisotropy data, which requires the assumption of a primordial spatial inhomogeneity power spectrum. As mentioned above, the only currently known physically motivated power spectra in non-flat models are untilted power spectra generated by slow-roll inflation. Such power spectra might not be general enough, so the CMB anisotropy data constraints on spatial curvature derived using these power spectra could be misleading. It is therefore of great importance to constrain spatial curvature and dark energy dynamics using non-CMB data that does not require the assumption of a primordial spatial inhomogeneity power spectrum. For recent studies along these lines, see [Farooq et al. \(2015\)](#), [Chen et al. \(2016\)](#), [Yu & Wang \(2016\)](#), [Farooq et al. \(2017\)](#), [Wei & Wu \(2017\)](#), [Rana et al. \(2017\)](#), [Yu et al. \(2018\)](#), [Qi et al. \(2018\)](#), [Ryan et al. \(2018\)](#), [Park & Ratra \(2018c\)](#), [Mukherjee et al. \(2019\)](#), [DES Collaboration \(2018a\)](#), [Zheng et al. \(2019\)](#), and [Ruan et al. \(2019\)](#).⁴

We recently used Hubble parameter and baryon acoustic oscillation (BAO) measurements to constrain spatial curvature and dark energy dynamics ([Ryan et al. 2018](#)).⁵ Here we improve upon and extend the analyses of [Ryan et al. \(2018\)](#). Compared to [Ryan et al. \(2018\)](#) we:

- Consider a sixth cosmological model, flat Λ CDM.
- Update a BAO measurement.
- More accurately compute the size of the sound horizon at the drag epoch for the BAO constraints.
- Treat the Hubble constant H_0 as an adjustable parameter to be determined by the data we use.
- Use milliarcsecond quasar angular size versus redshift data ([Cao et al. 2017b](#)), alone and in combination with $H(z)$ and BAO data, to constrain cosmological parameters.

We note that, in our analyses here, we make use of the baryon density determined from the Planck 2015 TT + lowP + lensing CMB anisotropy data ([Planck Collaboration](#)

the data compilation and non-flat model used. However, the tilted flat Λ CDM model is not nested inside any of the three untilted non-flat models, so it is not possible to convert these $\Delta\chi^2$ values to relative goodness-of-fit probabilities ([Ooba et al. 2018b,c,d](#); [Park & Ratra 2018b,a,d](#)).

³ For studies of other spatially-flat dynamical dark energy models that fit the data better than does flat Λ CDM, see [Zhang et al. \(2017a\)](#), [Wang et al. \(2018\)](#), and [Zhang et al. \(2018\)](#).

⁴ For possible constraints on spatial curvature from future data, see [Witzemann et al. \(2018\)](#) and [Wei \(2018\)](#).

⁵ Hubble parameter data span a large enough redshift range to be able to detect and study the transition from early matter dominated cosmological deceleration to the current dark energy dominated accelerated expansion (see, e.g., [Farooq & Ratra 2013](#); [Farooq et al. 2013](#); [Moresco et al. 2016a](#); [Farooq et al. 2017](#); [Jesus et al. 2018](#); [Gómez-Valent 2018](#)). For other uses of Hubble parameter data, see [Chen & Ratra \(2011b\)](#), [Chen et al. \(2015\)](#), [Anagnostopoulos & Basilakos \(2018\)](#), [Mamon & Bamba \(2018\)](#), [Geng et al. \(2018\)](#), and [Liu et al. \(2018\)](#).

[2016](#)), as computed in each of the six cosmological models we consider by [Park & Ratra \(2018b,a,d\)](#), so strictly speaking our constraints are not completely independent of the CMB anisotropy data. That said, the baryon density determined from the CMB anisotropy data in the spatially flat models is very consistent with the baryon density determined from deuterium abundance measurements, though it is a little less consistent with these measurements in the non-flat models ([Penton et al. 2018](#)).

The new data that we incorporate in this paper consists of a set of measurements of angular size from [Cao et al. \(2017b\)](#).⁶ Measurements of the milliarcsecond angular size of distant radio sources, from data compiled in [Gurvits et al. \(1999\)](#), have been used in the past to constrain cosmological parameters; see [Vishwakarma \(2001\)](#), [Lima & Alcaniz \(2002\)](#), [Zhu & Fujimoto \(2002\)](#), and [Chen & Ratra \(2003\)](#). There is, however, reason to doubt some of these earlier findings. Angular size measurements are only useful if radio sources are standard rulers, as accurate knowledge of the characteristic linear size l_m of the ruler is necessary to convert measurements of the angular size distance into measurements of the angular size, and the estimates of l_m used by [Vishwakarma \(2001\)](#), [Lima & Alcaniz \(2002\)](#), and [Zhu & Fujimoto \(2002\)](#) were inaccurate. To account for the uncertainty in the characteristic linear size l_m , [Chen & Ratra \(2003\)](#) marginalized over l_m , finding only weak constraints on the cosmological parameters they studied from the angular size data. More recent studies, such as [Cao et al. \(2017a\)](#) and [Cao et al. \(2017b\)](#), based on a sample of 120 intermediate-luminosity quasars recently compiled by [Cao et al. \(2017b\)](#), have more precisely calibrated l_m , and these angular size versus redshift data have been used to constrain cosmological parameters ([Cao et al. 2017b](#); [Li et al. 2017](#); [Qi et al. 2017](#); [Xu et al. 2018](#)). Here we use these data, in conjunction with measurements of $H(z)$ and BAO distance measurements, to constrain cosmological parameters. We find that when the QSO angular size versus redshift data are used in conjunction with the $H(z)$ + BAO data combination, cosmological parameter constraints tighten a bit. We also confirm, as described below, that the QSO data have a large reduced $\chi^2 \sim 3$.

From the $H(z)$ + BAO data combination, we measure a Hubble constant H_0 that is very consistent with the $H_0 = 68 \pm 2.8 \text{ km s}^{-1} \text{ Mpc}^{-1}$ median statistics estimate ([Chen & Ratra 2011a](#)) but is a model-dependent 2.2σ to 3.5σ (from the quadratic sum of the error bars) lower than the local expansion rate measurement of $H_0 = 73.48 \pm 1.66 \text{ km s}^{-1} \text{ Mpc}^{-1}$ ([Riess et al. 2018](#)). In the non-flat Λ CDM model these data are consistent with flat spatial hypersurfaces, while they favor closed geometry at 1.3σ and 1.4σ in the non-flat XCDM parametrization and non-flat ϕ CDM model, respectively. In the dynamical dark energy models, both flat and non-flat, these data favor dark energy dynamics over a Λ , from a little above 1σ to a little above 2σ .

In [Sec. 2](#) we describe the models that we study in this paper, [Sec. 3](#) summarizes the data we use, [Sec. 4](#) describes

⁶ For other angular size versus redshift data compilations and constraints, see [Daly & Guerra \(2002\)](#), [Podariu et al. \(2003\)](#), [Bonamente et al. \(2006\)](#), and [Chen & Ratra \(2012\)](#).

our methods, Sec. 5 describes our results, and we conclude in Sec. 6.

2 MODELS

We consider three pairs of dark energy models: the spatially-flat and non-flat models in which dark energy is a cosmological constant Λ (flat and non-flat Λ CDM), a dynamical X -fluid with an energy density ρ_X (flat and non-flat XCDM), or a dynamical scalar field ϕ (flat and non-flat ϕ CDM).

In the Λ CDM models the Hubble parameter as a function of redshift z obeys the Friedmann equation

$$H(z) = H_0 \sqrt{\Omega_{m0}(1+z)^3 + \Omega_{k0}(1+z)^2 + \Omega_\Lambda}, \quad (1)$$

where H_0 is the Hubble constant, Ω_{m0} and Ω_{k0} are the current values of the non-relativistic matter and spatial curvature energy density parameters, and Ω_Λ is the cosmological constant energy density parameter. Conventionally the parameters of the non-flat Λ CDM model are chosen to be $(H_0, \Omega_{m0}, \Omega_\Lambda)$, where $\Omega_{k0} = 1 - \Omega_{m0} - \Omega_\Lambda$, while for the standard spatially-flat Λ CDM model (Peebles 1984) the conventional choice is (H_0, Ω_{m0}) with $\Omega_{k0} = 0$ so $\Omega_\Lambda = 1 - \Omega_{m0}$.

The XCDM parametrization is widely used to describe dynamical dark energy. It is physically incomplete because it is based on an ideal, spatially homogeneous X -fluid with equation of state relating the pressure and energy density, $p_X = w_X \rho_X$, and negative equation of state parameter w_X . This renders it incapable of sensibly describing the evolution of spatial inhomogeneities. When $w_X = -1$, the XCDM parametrization reduces to the physically complete Λ CDM model. In the XCDM parametrization the Hubble parameter is

$$H(z) = H_0 \sqrt{\Omega_{m0}(1+z)^3 + \Omega_{k0}(1+z)^2 + \Omega_{X0}(1+z)^{3(1+w_X)}}, \quad (2)$$

where Ω_{X0} is the current value of the X -fluid energy density parameter. In the non-flat XCDM case the conventional parameters are $(H_0, \Omega_{m0}, \Omega_{k0}, w_X)$, while for flat XCDM, $\Omega_{k0} = 0$, in which case the parameters are (H_0, Ω_{m0}, w_X) .

Dynamical dark energy is modelled as a scalar field, ϕ , in the physically complete ϕ CDM model (Peebles & Ratra 1988, Ratra & Peebles 1988, Pavlov et al. 2013).⁷ Here the scalar field potential energy density is

$$V = \frac{1}{2} \kappa m_P^2 \phi^{-\alpha}, \quad (3)$$

where m_P is the Planck mass and

$$\kappa = \frac{8}{3} \left(\frac{\alpha+4}{\alpha+2} \right) \left[\frac{2}{3} \alpha(\alpha+2) \right]^{\alpha/2} \quad (4)$$

(we have fixed a typo in Eq. 4 that was present in Ryan et al. 2018). In the ϕ CDM model α is an adjustable parameter; in the limit $\alpha \rightarrow 0$, ϕ CDM reduces to Λ CDM. The dynamics of the ϕ CDM model is more complicated than the

⁷ For discussions of the ϕ CDM model see Samushia et al. (2007), Yashar et al. (2009), Samushia & Ratra (2010), Samushia et al. (2010), Avsajanishvili et al. (2015), Zhai et al. (2017), Sangwan et al. (2018), Yang et al. (2018), Sola et al. (2018), Tosone et al. (2018), and Singh et al. (2018).

dynamics of either the Λ CDM model or XCDM parametrization, because the scalar field ϕ is a dynamical variable with its own equation of motion. The ϕ CDM model dynamics is governed by two coupled non-linear ordinary differential equations, the first being the equation of motion for the spatially-homogeneous part of the scalar field

$$\ddot{\phi} + \frac{3\dot{a}}{a} \dot{\phi} - \frac{1}{2} \alpha \kappa m_P^2 \phi^{-\alpha-1} = 0, \quad (5)$$

and the second being the Friedmann equation

$$\left(\frac{\dot{a}}{a} \right)^2 = \frac{8\pi G}{3} (\rho_m + \rho_\phi) - \frac{k}{a^2}. \quad (6)$$

Here the scalar field energy density is

$$\rho_\phi = \frac{1}{2} \dot{\phi}^2 + V, \quad (7)$$

which implies a scalar field energy density parameter

$$\Omega_\phi(z, \alpha) = \frac{8\pi G \rho_\phi}{3H_0^2}, \quad (8)$$

where $\Omega_\phi(z, \alpha)$ is not a simple function of z , and must be reconstructed from a numerical solution of eqs. (5) and (6). In the general non-flat case, the Hubble rate can be written

$$H(z) = H_0 \sqrt{\Omega_{m0}(1+z)^3 + \Omega_{k0}(1+z)^2 + \Omega_\phi(z, \alpha)}, \quad (9)$$

and the conventional choice of parameters is $(H_0, \Omega_{m0}, \Omega_{k0}, \alpha)$, while in the spatially-flat case the parameters are $(H_0, \Omega_{m0}, \alpha)$.

3 DATA

We use a combination of 120 quasar angular size measurements ("QSO"), 31 expansion rate measurements (" $H(z)$ "), and 11 baryon acoustic oscillation observations ("BAO") to constrain our models. The $H(z)$ and BAO data are identical to the data compiled in Ryan et al. (2018) with one exception: in Ryan et al. (2018) we used the preprint value of the measurement from Ata et al. (2018), which we update in this paper to match the measurement in the published version (see Table 1 here for the updated BAO data). See Ryan et al. (2018) for a discussion of the $H(z)$ data. Our analysis of the BAO data in this paper differs from that of Ryan et al. (2018), as discussed below.

The BAO measurements collected in Table 1 are expressed in terms of the transverse co-moving distance

$$D_M(z) = \begin{cases} D_C(z) & \text{if } \Omega_{k0} = 0, \\ \frac{c}{H_0 \sqrt{|\Omega_{k0}|}} \sinh \left[\sqrt{|\Omega_{k0}|} H_0 D_C(z) / c \right] & \text{if } \Omega_{k0} > 0, \\ \frac{c}{H_0 \sqrt{|\Omega_{k0}|}} \sin \left[\sqrt{|\Omega_{k0}|} H_0 D_C(z) / c \right] & \text{if } \Omega_{k0} < 0, \end{cases} \quad (10)$$

the Hubble distance

$$D_H(z) = \frac{c}{H(z)}, \quad (11)$$

the volume-averaged angular diameter distance

$$D_V(z) = \left[\frac{cz}{H_0} \frac{D_M^2(z)}{E(z)} \right]^{1/3}, \quad (12)$$

and the line-of-sight comoving distance

$$D_C(z) \equiv \frac{c}{H_0} \int_0^z \frac{dz'}{E(z')}, \quad (13)$$

where c is the speed of light and $E(z) \equiv H(z)/H_0$ (Hogg 1999; Farooq 2013).

All measurements listed in Table 1 are scaled by the size of the sound horizon at the drag epoch r_s . This quantity is (see Eisenstein & Hu 1998 for a derivation)

$$r_s = \frac{2}{3k_{\text{eq}}} \sqrt{\frac{6}{R_{\text{eq}}}} \ln \left[\frac{\sqrt{1+R_d} + \sqrt{R_d + R_{\text{eq}}}}{1 + \sqrt{R_{\text{eq}}}} \right], \quad (14)$$

where $R_d \equiv R(z_d)$ and $R_{\text{eq}} \equiv R(z_{\text{eq}})$ are the values of R , the ratio of the baryon to photon momentum density

$$R = \frac{3\rho_b}{4\rho_\gamma}, \quad (15)$$

at the drag and matter-radiation equality redshifts z_d and z_{eq} , respectively, and k_{eq} is the particle horizon wavenumber at the matter-radiation equality epoch.

To compute r_s as a function of our model parameters, we use the fitting formula presented in Eisenstein & Hu (1998). This calculation also requires $\Omega_b h^2$ as input, and in Ryan et al. (2018) we used $\Omega_b h^2 = 0.02227$ for all models considered. It is more accurate, however, to use the different values of $\Omega_b h^2$ computed by Park & Ratra (2018a,b,d) for each model from the Planck 2015 TT + lowP + lensing CMB anisotropy data (Planck Collaboration 2016). This is because the values of $\Omega_b h^2$ estimated from CMB anisotropy data are model dependent, and vary significantly between the spatially-flat and non-flat inflation models (Park & Ratra 2018a). The values of $\Omega_b h^2$ that we use are collected in Table 2. We do not list the small uncertainties in $\Omega_b h^2$, which we do not account for in our analyses.

Our method of scaling the sound horizon in this paper differs from the method used in Ryan et al. (2018). For studies that scale their measurements by $r_{s,\text{fid}}/r_s$, we use the fitting formula of Eisenstein & Hu (1998) to compute both r_s and $r_{s,\text{fid}}$. For $r_{s,\text{fid}}$ we use the parameters ($\Omega_{m0}, H_0, \Omega_b h^2$) of the fiducial cosmology adopted in the paper in which the measurement is reported. For measurements scaled only by r_s , we again use the fitting formula of Eisenstein & Hu (1998), but we modify it with a multiplicative scaling factor $147.60 \text{ Mpc}/r_{s,\text{Planck}}$, where 147.60 Mpc is the value of the sound horizon from Table 4, column 3 of Planck Collaboration (2016), and $r_{s,\text{Planck}}$ is the output of the sound horizon fitting formula from Eisenstein & Hu (1998) when it takes the best-fitting values of ($\Omega_{m0}, H_0, \Omega_b h^2$) from Planck Collaboration (2016) as input.⁸ We do this because the output of the fitting formula in Eisenstein & Hu (1998) deviates by a few per cent from CAMB's output; the scaling factor ensures that $r_s = 147.60 \text{ Mpc}$ when ($\Omega_{m0}, H_0, \Omega_b h^2$) take their best-fitting values found by Planck Collaboration (2016). We believe that these modifications to the output of the fitting formula result in more accurate determinations of the size of the sound horizon than the scaling employed in Ryan et al. (2018).

Recently, Cao et al. (2017a) found that compact structures in intermediate-luminosity radio quasars could serve

⁸ We thank C.-G. Park for suggesting this.

as standard cosmological rulers. Our QSO data come from a newly compiled sample of these standard rulers from observations of 120 intermediate-luminosity quasars taken over a redshift range of $0.46 < z < 2.76$, with angular sizes $\theta_{\text{obs}}(z)$ and redshifts z listed in Table 1 of Cao et al. (2017b). The corresponding theoretical predictions for the angular sizes can be obtained via

$$\theta_{\text{th}}(z) = \frac{l_m}{D_A(z)}, \quad (16)$$

where $l_m = 11.03 \pm 0.25 \text{ pc}$ is the intrinsic linear size of the ruler (see Cao et al. 2017b), and

$$D_A(z) = \frac{D_M(z)}{1+z} \quad (17)$$

is the angular diameter distance at redshift z (see Hogg 1999).

4 DATA ANALYSIS METHODS

We use the χ^2 statistic to find the best-fitting parameter values and limits for a given model. Most of the data points we use are uncorrelated, so

$$\chi^2(p) = \sum_{i=1}^N \frac{[A_{\text{th}}(p; z_i) - A_{\text{obs}}(z_i)]^2}{\sigma_i^2}. \quad (18)$$

Here p is the set of model parameters, for example $p = (H_0, \Omega_{m0})$ in the flat Λ CDM model, z_i is the redshift at which the measured value is $A_{\text{obs}}(z_i)$ with one standard deviation uncertainty σ_i , and $A_{\text{th}}(p; z_i)$ is the predicted value computed in the model under consideration. The χ^2 expression in eq. (18) holds for the $H(z)$ measurements listed in Table 2 of Ryan et al. (2018) and the BAO measurements listed in the last five lines of Table 1 here.

The measurements in the first six lines of Table 1 are correlated, in which case χ^2 is given by

$$\chi^2(p) = [\mathbf{A}_{\text{th}}(p) - \mathbf{A}_{\text{obs}}]^T \mathbf{C}^{-1} [\mathbf{A}_{\text{th}}(p) - \mathbf{A}_{\text{obs}}] \quad (19)$$

where \mathbf{C}^{-1} is the inverse of the covariance matrix $\mathbf{C} =$

$$\begin{bmatrix} 624.707 & 23.729 & 325.332 & 8.34963 & 157.386 & 3.57778 \\ 23.729 & 5.60873 & 11.6429 & 2.33996 & 6.39263 & 0.968056 \\ 325.332 & 11.6429 & 905.777 & 29.3392 & 515.271 & 14.1013 \\ 8.34963 & 2.33996 & 29.3392 & 5.42327 & 16.1422 & 2.85334 \\ 157.386 & 6.39263 & 515.271 & 16.1422 & 1375.12 & 40.4327 \\ 3.57778 & 0.968056 & 14.1013 & 2.85334 & 40.4327 & 6.25936 \end{bmatrix} \quad (20)$$

which we extracted from the source files of Alam et al. (2017).⁹

For the QSO data (Cao et al. 2017b) we use

$$\chi^2(p) = \sum_{i=1}^N \left[\frac{\theta_{\text{th}}(p; z_i) - \theta_{\text{obs}}(z_i)}{\sigma_i + 0.1\theta_{\text{obs}}(z_i)} \right]^2, \quad (21)$$

where $\theta_{\text{th}}(p; z_i)$ is the model-predicted value of the angular

⁹ In Ryan et al. (2018) we extracted the covariance matrix from the full covariance matrix presented in Alam et al. (2017) by simply deleting the rows and columns containing $f\sigma_8$ data from Table 8 of that paper, but this procedure is less accurate than what we have done here.

Table 1. BAO data. $D_M(r_{s,\text{fid}}/r_s)$ and $D_V(r_{s,\text{fid}}/r_s)$ have units of Mpc, while $H(z)(r_s/r_{s,\text{fid}})$ has units of $\text{km s}^{-1}\text{Mpc}^{-1}$ and r_s and $r_{s,\text{fid}}$ have units of Mpc.

z	Measurement	Value	σ	Ref.
0.38	$D_M(r_{s,\text{fid}}/r_s)$	1518	22	Alam et al. (2017)
0.38	$H(z)(r_s/r_{s,\text{fid}})$	81.5	1.9	Alam et al. (2017)
0.51	$D_M(r_{s,\text{fid}}/r_s)$	1977	27	Alam et al. (2017)
0.51	$H(z)(r_s/r_{s,\text{fid}})$	90.4	1.9	Alam et al. (2017)
0.61	$D_M(r_{s,\text{fid}}/r_s)$	2283	32	Alam et al. (2017)
0.61	$H(z)(r_s/r_{s,\text{fid}})$	97.3	2.1	Alam et al. (2017)
0.106	r_s/D_V	0.336	0.015	Beutler et al. (2011)
0.15	$D_V(r_{s,\text{fid}}/r_s)$	664	25	Ross et al. (2015)
1.52	$D_V(r_{s,\text{fid}}/r_s)$	3843	147	Ata et al. (2018)
2.33	$\frac{(D_H)^{0.7}(D_M)^{0.3}}{r_s}$	13.94	0.35	Bautista et al. (2017)
2.36	$c/(r_s H(z))$	9.0	0.3	Font-Ribera et al. (2014)

Table 2. Baryon density for different models.

Model	$\Omega_b h^2$	Ref.
Flat Λ CDM	0.02225	Park & Ratra (2018a)
Nonflat Λ CDM	0.02305	Park & Ratra (2018a)
Flat XCDM	0.02229	Park & Ratra (2018b)
Nonflat XCDM	0.02305	Park & Ratra (2018b)
Flat ϕ CDM	0.02221	Park & Ratra (2018d)
Nonflat ϕ CDM	0.02303	Park & Ratra (2018d)

size, $\theta_{\text{obs}}(z_i)$ is the measured angular size at redshift z_i , and σ_i is the uncertainty on the measurement made at redshift z_i . The term proportional to $\theta_{\text{obs}}(z_i)$ in the denominator is added to σ_i in order to account for systematic uncertainties in the angular size measurements (see the discussion of this point in the first paragraph of Sec. 3 of Cao et al. 2017b).

To determine constraints on the model parameters, we use the likelihood

$$\mathcal{L}(p) = e^{-\chi(p)^2/2}. \quad (22)$$

We are interested in presenting two-dimensional confidence contour plots and one-dimensional likelihoods. To do this, for the models with more than two parameters, we marginalize over the parameters in turn to get two-dimensional likelihoods. For example, in the non-flat Λ CDM model one of the two-dimensional likelihoods we compute is

$$\mathcal{L}(\Omega_{m0}, \Omega_\Lambda) = \int \mathcal{L}(\Omega_{m0}, H_0, \Omega_\Lambda) dH_0, \quad (23)$$

where we integrate over the 50 to 85 $\text{km s}^{-1} \text{Mpc}^{-1}$ range with a flat prior.¹⁰ We then plot the isocontours of

¹⁰ In Ryan et al. (2018) we used two H_0 priors, gaussian with central values and error bars of $\bar{H}_0 \pm \sigma_{H_0} = 68 \pm 2.8 \text{ km s}^{-1} \text{Mpc}^{-1}$ (Chen & Ratra 2011a) and $\bar{H}_0 \pm \sigma_{H_0} = 73.24 \pm 1.74 \text{ km s}^{-1} \text{Mpc}^{-1}$ (Riess et al. 2016). Here we are instead treating H_0 as an adjustable parameter to be determined from the data we use.

$\chi^2(\Omega_{m0}, \Omega_\Lambda) = -2\ln\mathcal{L}(\Omega_{m0}, \Omega_\Lambda)$ in the Ω_{m0} - Ω_Λ subspace of the total parameter space.

To obtain the one-dimensional likelihood distribution as a function of a given parameter within a model, we marginalize the likelihood distribution over the other parameters. The marginalization ranges that we use for the parameters of each model are listed in Tables 4, 6, and 8; for all parameters we assume a flat prior distribution, and we use a step size of $\Delta p = 0.01$. The only exception to this is the step size of H_0 in non-flat XCDM and non-flat ϕ CDM, for which we use $\Delta H_0 = 0.1 \text{ km s}^{-1} \text{Mpc}^{-1}$ (to reduce computation time). The best-fitting value of a parameter p , after marginalization, is that value \bar{p} which maximizes the one-dimensional likelihood function. To determine the confidence limits r_n^\pm on either side of \bar{p} , we compute

$$\frac{\int_{\bar{p}}^{r_n^+} \mathcal{L}(p) dp}{\int_{\bar{p}}^{\pm\infty} \mathcal{L}(p) dp} = \sigma_n \quad (24)$$

where $\sigma_{1,2} = 0.6827, 0.9545$ and r_n^+, r_n^- are the upper and lower confidence limits out to σ_n , respectively.

In addition to the χ^2 statistic, we also use the Akaike Information Criterion

$$AIC \equiv \chi_{\min}^2 + 2k \quad (25)$$

and the Bayes Information Criterion

$$BIC \equiv \chi_{\min}^2 + k \ln N \quad (26)$$

(Liddle 2007), where χ_{\min}^2 is the minimum value of χ^2 in the given model, k is the number of parameters in the model, and N is the number of data points. The AIC and BIC penalize models with a greater number of parameters compared to those with fewer parameters, and as such they can be used to compare the effectiveness of the fits of models with different numbers of parameters.

5 RESULTS

5.1 $H(z)$ + BAO constraints

We present our results for the $H(z)$ + BAO data combination first (i.e. without the QSO data). We have broken these results into three categories: $H(z)$ data only with 31 measurements, $H(z)$ + 2 BAO with 33 measurements, and $H(z)$ + All BAO with 42 measurements. The results in the $H(z)$ only category use only the $H(z)$ data listed in Table 2 of [Ryan et al. \(2018\)](#) and appear in Figs. A1-A6 as two-dimensional dotted black likelihood contours and one-dimensional dotted black likelihood distributions. The results in the $H(z)$ + 2 BAO category use the $H(z)$ data from [Ryan et al. \(2018\)](#) plus the data points from the last two lines of Table 1 and appear in Figs. A1-A6 as two-dimensional dashed black likelihood contours and one-dimensional dashed black likelihood distributions. The results in the $H(z)$ + All BAO category use all of the $H(z)$ and BAO measurements and appear in Figs. A1-A6 as two-dimensional solid black likelihood contours and one-dimensional solid black likelihood distributions.

The best-fitting values of the parameters of our models, from the unmarginalized two-, three-, or four-dimensional likelihood, for every data combination we consider, are listed in Tables 3, 5, and 7. These tables also list the number of degrees of freedom, ν , and the values of χ^2 , AIC , and BIC that correspond to the best-fitting parameters. The marginalized, one-dimensional best-fitting values of our model parameters, along with their 1σ and 2σ ranges, for every data combination we consider, are listed in Tables 4, 6, and 8.

The last two high redshift data points, at $z = 2.33$ and $z = 2.36$ in Table 1, include radial BAO data that measure the expansion rate $H(z)$. It is of interest to examine the effects of adding these to the other $H(z)$ data we use (listed in Table 2 of [Ryan et al. 2018](#)) because these higher- z expansion rate measurements are approximately 2σ discrepant with the predictions of the standard flat Λ CDM model normalized to fit the Planck CMB anisotropy measurements (see Fig. 11 of [Planck Collaboration 2018](#)). Here, however, we find that the differences between the best-fitting parameters in the $H(z)$ and $H(z)$ + 2 BAO cases are usually less than 1σ and never more than 1.15σ (see Tables 4, 6, and 8).

The flat Λ CDM model (with two free parameters, H_0 and Ω_{m0}) two-dimensional χ^2 confidence contours and one-dimensional normalized likelihood distributions are plotted in Fig. A1. In Figs. A2-A6 we present our results for the non-flat Λ CDM model, the flat and non-flat XCDM parametrizations, and the flat and non-flat ϕ CDM models. Comparing the $H(z)$ only, $H(z)$ + 2 BAO, and $H(z)$ + All BAO constraints in Figs. A1-A6 and Tables 3-8, we see no indication of any significant inconsistency between the results derived from these different $H(z)$ and BAO combinations. The constraints are more restrictive for the $H(z)$ + All BAO combination, which we now consider in more detail.

When it is measured using the $H(z)$ + All BAO data combination, Ω_{m0} has consistent best-fitting values, and tight confidence limits, across the models we studied (see Tables 4, 6, and 8). For the flat and non-flat Λ CDM models, $\Omega_{m0} = 0.31^{+0.01}_{-0.02}$ and $\Omega_{m0} = 0.30^{+0.02}_{-0.01}$, respectively. For flat XCDM and flat ϕ CDM we find $\Omega_{m0} = 0.31^{+0.02}_{-0.01}$, while non-flat XCDM and non-flat ϕ CDM favor the slightly larger values $\Omega_{m0} = 0.33^{+0.02}_{-0.02}$ and $\Omega_{m0} = 0.32^{+0.02}_{-0.02}$, respectively. Be-

cause our Ω_{m0} step size is 0.01, the 1σ error bars on Ω_{m0} that we list here are probably somewhat inaccurate. The data, however, do determine Ω_{m0} fairly precisely, with the error bars increasing a bit as the number of model parameters increase, as expected. These Ω_{m0} estimates are in reasonable agreement with those made by [Park & Ratra \(2018c\)](#) from a similar compilation of $H(z)$ and BAO data.

The measurements of H_0 vary a bit less across the models we studied. For flat (non-flat) Λ CDM we measure $H_0 = 67.78^{+0.91}_{-0.87} (67.16^{+2.40}_{-2.34})$ km s⁻¹ Mpc⁻¹, while for flat (non-flat) XCDM $H_0 = 65.16^{+2.45}_{-2.20} (65.5^{+2.4}_{-2.2})$ km s⁻¹ Mpc⁻¹, and for flat (non-flat) ϕ CDM we find $H_0 = 64.94^{+1.76}_{-2.10} (66.0^{+2.4}_{-2.2})$ km s⁻¹ Mpc⁻¹, all with 1σ error bars. Our step size is $\Delta H_0 = 0.01$ km s⁻¹ Mpc⁻¹ for the flat models and non-flat Λ CDM, which we increased to $\Delta H_0 = 0.1$ km s⁻¹ Mpc⁻¹ for the non-flat XCDM and ϕ CDM cases, so the H_0 error bars are more accurate than those of the Ω_{m0} measurements. These six measured H_0 values are mutually quite consistent. Aside from the flat Λ CDM case, the H_0 central values and limits are very consistent with those found from a similar $H(z)$ + BAO data compilation in [Park & Ratra \(2018c\)](#). Unlike here where we fix $\Omega_b h^2$ to the values obtained by [Park & Ratra \(2018a,b,d\)](#), [Park & Ratra \(2018c\)](#) allow the baryonic matter density parameter to vary, so the [Park & Ratra \(2018c\)](#) models have an additional free parameter compared to our models; this will have a bigger effect in the flat Λ CDM case which has the fewest parameters. These H_0 measurements are more consistent with the recent median statistics estimate of $H_0 = 68 \pm 2.8$ km s⁻¹ Mpc⁻¹ ([Chen & Ratra 2011a](#)), and with earlier median statistics estimates ([Gott et al. 2001](#), [Chen et al. 2003](#))¹¹ than with the recent measurement of $H_0 = 73.48 \pm 1.66$ km s⁻¹ Mpc⁻¹ determined from the local expansion rate ([Riess et al. 2018](#)).¹² As a comparison, both our highest and lowest H_0 measurements (those of non-flat Λ CDM and flat ϕ CDM, respectively) are within 1σ of the measurement made in [Chen & Ratra \(2011a\)](#), relative to the error bars of that measurement, but they are 2.2σ (non-flat Λ CDM) and 3.5σ (flat ϕ CDM) lower than the [Riess et al. \(2018\)](#) measurement (here σ is the quadrature sum of the two measurement error bars, and these two cases span the range of differences).

As for spatial curvature, we find some evidence in favor of non-flat spatial hypersurfaces, although this evidence is fairly weak. For non-flat Λ CDM, we measure $\Omega_{k0} = 0.03^{+0.07}_{-0.08}$, with 1σ error bars, consistent with spatial flatness (see Table 6). For the non-flat XCDM parametrization and non-flat ϕ CDM model, we measure $\Omega_{k0} = -0.24^{+0.18}_{-0.26}$, and $\Omega_{k0} = -0.23^{+0.16}_{-0.15}$, respectively (1σ error bars). From these results we can see that non-flat XCDM and non-flat

¹¹ These H_0 measurements are also consistent with many other recent H_0 measurements ([Chen et al. 2017](#), [Wang et al. 2017](#), [Lin & Ishak 2017](#), [DES Collaboration 2018b](#), [da Silva & Cavalcanti 2018](#), [Gómez-Valent & Amendola 2018](#), [Planck Collaboration 2018](#), [Yu et al. 2018](#), [Zhang 2018](#), [Zhang & Huang 2018](#), [Ruan et al. 2019](#), [Zhang et al. 2019](#)).

¹² We note that other local expansion rate H_0 values are slightly lower, with slightly larger error bars. See, e.g., [Zhang et al. \(2017b\)](#), [Dhawan et al. \(2018\)](#), and [Fernández Arenas et al. \(2018\)](#).

Table 3. Best-fitting parameters of the flat Λ CDM model.

Data set	Ω_{m0}	H_0^a	ν	χ^2	AIC	BIC
$H(z)$ only	0.32	68.13	28	14.50	18.50	21.37
$H(z)$ + 2 BAO	0.27	69.29	30	17.76	21.76	24.75
$H(z)$ + All BAO	0.31	67.81	39	39.89	43.89	47.37
QSO	0.32	68.49	117	352.05	356.05	361.63
QSO + $H(z)$ + BAO	0.31	68.21	159	395.54	399.54	405.72

^a km s⁻¹Mpc⁻¹.

Table 4. Best-fitting parameters and 1σ and 2σ confidence intervals for the flat Λ CDM model.

Data set	Marginalization range ^a	Best-fitting	1σ	2σ
$H(z)$ only	$0.1 \leq \Omega_{m0} \leq 0.7$ $50 \leq H_0 \leq 85$	$\Omega_{m0} = 0.32$ $H_0 = 67.83$	$0.27 \leq \Omega_{m0} \leq 0.39$ $64.67 \leq H_0 \leq 70.86$	$0.22 \leq \Omega_{m0} \leq 0.47$ $61.44 \leq H_0 \leq 73.84$
$H(z)$ + 2 BAO	$0.1 \leq \Omega_{m0} \leq 0.7$ $50 \leq H_0 \leq 85$	$\Omega_{m0} = 0.27$ $H_0 = 69.13$	$0.23 \leq \Omega_{m0} \leq 0.32$ $66.11 \leq H_0 \leq 72.02$	$0.19 \leq \Omega_{m0} \leq 0.38$ $63.04 \leq H_0 \leq 74.87$
$H(z)$ + All BAO	$0.1 \leq \Omega_{m0} \leq 0.7$ $50 \leq H_0 \leq 85$	$\Omega_{m0} = 0.31$ $H_0 = 67.78$	$0.29 \leq \Omega_{m0} \leq 0.32$ $66.91 \leq H_0 \leq 68.69$	$0.28 \leq \Omega_{m0} \leq 0.34$ $66.04 \leq H_0 \leq 69.60$
QSO	$0.1 \leq \Omega_{m0} \leq 0.7$ $50 \leq H_0 \leq 85$	$\Omega_{m0} = 0.31$ $H_0 = 67.55$	$0.23 \leq \Omega_{m0} \leq 0.47$ $62.34 \leq H_0 \leq 72.33$	$0.16 \leq \Omega_{m0} \leq 0.63$ $58.17 \leq H_0 \leq 76.83$
QSO + $H(z)$ + BAO	$0.1 \leq \Omega_{m0} \leq 0.7$ $50 \leq H_0 \leq 85$	$\Omega_{m0} = 0.31$ $H_0 = 68.18$	$0.30 \leq \Omega_{m0} \leq 0.33$ $67.49 \leq H_0 \leq 68.88$	$0.29 \leq \Omega_{m0} \leq 0.34$ $66.80 \leq H_0 \leq 69.59$

^a H_0 has units of km s⁻¹Mpc⁻¹.

Table 5. Best-fitting parameters of the three-parameter models

Model	Data set	Ω_{m0}	Ω_Λ	w_X	α	H_0^a	ν	χ^2	AIC	BIC
Non-flat Λ CDM	$H(z)$ only	0.36	0.77	-	-	69.08	27	14.46	20.46	24.76
	$H(z)$ + 2 BAO	0.43	0.93	-	-	70.81	29	14.73	20.73	25.22
	$H(z)$ + All BAO	0.30	0.67	-	-	67.24	38	39.36	45.36	50.57
	QSO	0.27	1	-	-	74.62	116	351.30	357.30	365.66
	QSO + $H(z)$ + BAO	0.31	0.70	-	-	68.75	158	391.84	397.84	407.10
Flat XCDM	$H(z)$ only	0.32	-	-1.26	-	71.05	27	14.36	20.36	24.66
	$H(z)$ + 2 BAO	0.27	-	-1.10	-	70.79	29	17.60	23.60	28.09
	$H(z)$ + All BAO	0.31	-	-0.87	-	65.08	38	38.34	44.34	49.55
	QSO	0.27	-	-1.97	-	81.22	116	351.84	357.84	366.20
	QSO + $H(z)$ + BAO	0.32	-	-0.91	-	66.56	158	391.60	397.60	406.86
Flat ϕ CDM	$H(z)$ only	0.32	-	-	0.01	68.08	27	14.50	20.50	24.80
	$H(z)$ + 2 BAO	0.27	-	-	0.01	69.22	29	17.80	23.80	28.29
	$H(z)$ + All BAO	0.31	-	-	0.34	65.40	38	38.65	44.65	49.86
	QSO	0.32	-	-	0.01	68.44	116	352.05	358.05	366.41
	QSO + $H(z)$ + BAO	0.32	-	-	0.22	66.75	158	391.88	397.88	407.14

^a km s⁻¹Mpc⁻¹.

ϕ CDM favor closed spatial hypersurfaces at 1.3σ and 1.4σ , respectively. For these three cases, using a similar $H(z)$ and BAO data compilation, Park & Ratra (2018c) find $\Omega_{k0} = -0.086 \pm 0.078$, $\Omega_{k0} = -0.32 \pm 0.11$, and $\Omega_{k0} = -0.24 \pm 0.15$, respectively, favoring closed geometry at 1.1σ , 2.9σ , and 1.6σ , respectively. Our measurements of spatial curvature are also consistent with the results obtained by other groups, particularly with the model-independent constraints obtained by Yu & Wang (2016), Rana et al. (2017), Wei & Wu (2017), Yu et al. (2018), and Ruan et al. (2019). We find some

disagreement, however, with the model-independent studies conducted by Moresco et al. (2016b) and Zheng et al. (2019); when compared to the measurements of Ω_{k0} made by these groups, we only find consistency with our non-flat Λ CDM measurement of Ω_{k0} . Our non-flat XCDM and non-flat ϕ CDM measurements are not consistent with their measurements to 1σ , though they are consistent to 2σ , owing to the much larger error bars on our measurements.

Our results also show some evidence for dark energy dynamics, although like the evidence for

Table 6. Best-fitting parameters and 1σ and 2σ confidence intervals for the three-parameter models.

Model	Data set	Marginalization range ^a	Best-fitting	1σ	2σ
Non-flat Λ CDM	$H(z)$ only	$0.1 \leq \Omega_{m0} \leq 0.7$	$\Omega_{m0} = 0.34$	$0.21 \leq \Omega_{m0} \leq 0.46$	$0.12 \leq \Omega_{m0} \leq 0.57$
		$50 \leq H_0 \leq 85$	$H_0 = 67.36$	$63.83 \leq H_0 \leq 70.91$	$60.68 \leq H_0 \leq 74.22$
		$0.2 \leq \Omega_\Lambda \leq 1$	$\Omega_\Lambda = 0.75$	$0.44 \leq \Omega_\Lambda \leq 0.91$	$0.25 \leq \Omega_\Lambda \leq 0.99$
	$H(z) + 2$ BAO	$0.1 \leq \Omega_{m0} \leq 0.7$	$\Omega_{m0} = 0.40$	$0.31 \leq \Omega_{m0} \leq 0.49$	$0.23 \leq \Omega_{m0} \leq 0.59$
		$50 \leq H_0 \leq 85$	$H_0 = 69.80$	$66.80 \leq H_0 \leq 72.64$	$63.75 \leq H_0 \leq 75.44$
		$0.2 \leq \Omega_\Lambda \leq 1$	$\Omega_\Lambda = 0.92$	$0.79 \leq \Omega_\Lambda \leq 0.97$	$0.67 \leq \Omega_\Lambda \leq 1$
	$H(z) +$ All BAO	$0.1 \leq \Omega_{m0} \leq 0.7$	$\Omega_{m0} = 0.30$	$0.29 \leq \Omega_{m0} \leq 0.32$	$0.27 \leq \Omega_{m0} \leq 0.33$
		$50 \leq H_0 \leq 85$	$H_0 = 67.16$	$64.82 \leq H_0 \leq 69.56$	$62.50 \leq H_0 \leq 71.98$
		$0.2 \leq \Omega_\Lambda \leq 1$	$\Omega_\Lambda = 0.67$	$0.59 \leq \Omega_\Lambda \leq 0.74$	$0.51 \leq \Omega_\Lambda \leq 0.80$
	QSO	$0.1 \leq \Omega_{m0} \leq 0.7$	$\Omega_{m0} = 0.31$	$0.23 \leq \Omega_{m0} \leq 0.45$	$0.16 \leq \Omega_{m0} \leq 0.60$
		$50 \leq H_0 \leq 85$	$H_0 = 66.27$	$61.98 \leq H_0 \leq 71.93$	$58.50 \leq H_0 \leq 76.85$
		$0.2 \leq \Omega_\Lambda \leq 1$	N/A	N/A	N/A
QSO + $H(z) +$ BAO	$0.1 \leq \Omega_{m0} \leq 0.7$	$\Omega_{m0} = 0.31$	$0.30 \leq \Omega_{m0} \leq 0.32$	$0.29 \leq \Omega_{m0} \leq 0.34$	
	$50 \leq H_0 \leq 85$	$H_0 = 68.62$	$67.18 \leq H_0 \leq 70.05$	$65.74 \leq H_0 \leq 71.49$	
	$0.2 \leq \Omega_\Lambda \leq 1$	$\Omega_\Lambda = 0.70$	$0.64 \leq \Omega_\Lambda \leq 0.75$	$0.57 \leq \Omega_\Lambda \leq 0.80$	
Flat XCDM	$H(z)$ only	$0.1 \leq \Omega_{m0} \leq 0.7$	$\Omega_{m0} = 0.31$	$0.25 \leq \Omega_{m0} \leq 0.38$	$0.15 \leq \Omega_{m0} \leq 0.46$
		$50 \leq H_0 \leq 85$	$H_0 = 68.28$	$63.37 \leq H_0 \leq 75.26$	$59.31 \leq H_0 \leq 81.23$
		$-2 \leq w_X \leq 0$	$w_X = -1.2$	$-1.69 \leq w_X \leq -0.7$	$-1.95 \leq w_X \leq -0.41$
	$H(z) + 2$ BAO	$0.1 \leq \Omega_{m0} \leq 0.7$	$\Omega_{m0} = 0.27$	$0.23 \leq \Omega_{m0} \leq 0.32$	$0.19 \leq \Omega_{m0} \leq 0.38$
		$50 \leq H_0 \leq 85$	$H_0 = 70.65$	$66.62 \leq H_0 \leq 76.46$	$62.88 \leq H_0 \leq 81.98$
		$-2 \leq w_X \leq 0$	$w_X = -1.09$	$-1.52 \leq w_X \leq -0.88$	$-1.88 \leq w_X \leq -0.73$
	$H(z) +$ All BAO	$0.1 \leq \Omega_{m0} \leq 0.7$	$\Omega_{m0} = 0.31$	$0.30 \leq \Omega_{m0} \leq 0.33$	$0.28 \leq \Omega_{m0} \leq 0.35$
		$50 \leq H_0 \leq 85$	$H_0 = 65.16$	$62.96 \leq H_0 \leq 67.61$	$60.84 \leq H_0 \leq 70.18$
		$-2 \leq w_X \leq 0$	$w_X = -0.86$	$-0.98 \leq w_X \leq -0.77$	$-1.10 \leq w_X \leq -0.69$
	QSO	$0.1 \leq \Omega_{m0} \leq 0.7$	$\Omega_{m0} = 0.29$	$0.21 \leq \Omega_{m0} \leq 0.45$	$0.13 \leq \Omega_{m0} \leq 0.62$
		$50 \leq H_0 \leq 85$	$H_0 = 65.62$	$59.94 \leq H_0 \leq 75.17$	$55.51 \leq H_0 \leq 82.56$
		$-2 \leq w_X \leq 0$	$w_X = -1.41$	$-1.79 \leq w_X \leq -0.68$	$-1.97 \leq w_X \leq -0.30$
QSO + $H(z) +$ BAO	$0.1 \leq \Omega_{m0} \leq 0.7$	$\Omega_{m0} = 0.32$	$0.31 \leq \Omega_{m0} \leq 0.34$	$0.29 \leq \Omega_{m0} \leq 0.35$	
	$50 \leq H_0 \leq 85$	$H_0 = 66.54$	$64.72 \leq H_0 \leq 68.65$	$63.00 \leq H_0 \leq 70.89$	
	$-2 \leq w_X \leq 0$	$w_X = -0.91$	$-1.02 \leq w_X \leq -0.82$	$-1.14 \leq w_X \leq -0.73$	
Flat ϕ CDM	$H(z)$ only	$0.1 \leq \Omega_{m0} \leq 0.7$	$\Omega_{m0} = 0.27$	$0.20 \leq \Omega_{m0} \leq 0.35$	$0.15 \leq \Omega_{m0} \leq 0.44$
		$50 \leq H_0 \leq 85.01$	$H_0 = 65.23$	$62.17 \leq H_0 \leq 68.37$	$59.15 \leq H_0 \leq 71.53$
		N/A	N/A	N/A	N/A
	$H(z) + 2$ BAO	$0.1 \leq \Omega_{m0} \leq 0.7$	$\Omega_{m0} = 0.25$	$0.20 \leq \Omega_{m0} \leq 0.31$	$0.16 \leq \Omega_{m0} \leq 0.37$
		$50 \leq H_0 \leq 85.01$	$H_0 = 67.69$	$64.65 \leq H_0 \leq 70.69$	$61.40 \leq H_0 \leq 73.65$
		$0.01 \leq \alpha \leq 3$	$\alpha = 0.01$	$0.01 \leq \alpha \leq 0.57$	$0.01 \leq \alpha \leq 1.21$
	$H(z) +$ All BAO	$0.1 \leq \Omega_{m0} \leq 0.7$	$\Omega_{m0} = 0.31$	$0.30 \leq \Omega_{m0} \leq 0.33$	$0.28 \leq \Omega_{m0} \leq 0.35$
		$50 \leq H_0 \leq 85.01$	$H_0 = 64.94$	$62.84 \leq H_0 \leq 66.70$	$60.80 \leq H_0 \leq 68.15$
		$0.01 \leq \alpha \leq 3$	$\alpha = 0.35$	$0.14 \leq \alpha \leq 0.76$	$0.03 \leq \alpha \leq 1.23$
	QSO	$0.1 \leq \Omega_{m0} \leq 0.7$	$\Omega_{m0} = 0.26$	$0.18 \leq \Omega_{m0} \leq 0.44$	$0.12 \leq \Omega_{m0} \leq 0.62$
		$50 \leq H_0 \leq 85.01$	$H_0 = 64.31$	$59.80 \leq H_0 \leq 68.87$	$56.30 \leq H_0 \leq 73.30$
		N/A	N/A	N/A	N/A
QSO + $H(z) +$ BAO	$0.1 \leq \Omega_{m0} \leq 0.7$	$\Omega_{m0} = 0.32$	$0.31 \leq \Omega_{m0} \leq 0.34$	$0.29 \leq \Omega_{m0} \leq 0.35$	
	$50 \leq H_0 \leq 85.01$	$H_0 = 66.35$	$64.66 \leq H_0 \leq 67.58$	$63.02 \leq H_0 \leq 68.61$	
	$0.01 \leq \alpha \leq 3$	$\alpha = 0.21$	$0.08 \leq \alpha \leq 0.56$	$0.02 \leq \alpha \leq 0.94$	

^a H_0 has units of $\text{km s}^{-1}\text{Mpc}^{-1}$.

$|\Omega_{k0}| \neq 0$ it is also weak. For example, our measurements in the flat (non-flat) XCDM cases are $w_X = -0.86^{+0.09}_{-0.12}$ at 1σ ($w_X = -0.63^{+0.05+0.09}_{-0.15-0.35}$ at 1 and 2σ), which both favor quintessence-type dark energy, for which $w_X > -1$, over a Λ , though to different degrees of statistical

significance. The best-fitting value of w_X in the flat XCDM parametrization is only a little over 1σ away from $w_X = -1$ (which corresponds to flat Λ CDM), while the best-fitting value of w_X in the non-flat XCDM parametrization is a little more than 2σ away from $w_X = -1$ (non-flat Λ CDM

Table 7. Best-fitting parameters of the four-parameter models.

Model	Data set	Ω_{m0}	Ω_{k0}	w_X	α	H_0^a	ν	χ^2	AIC	BIC
Non-flat Λ CDM	$H(z)$ only	0.19	0.31	-2	-	73.4	26	14.12	22.12	27.86
	$H(z)$ + 2 BAO	0.44	-0.44	-0.85	-	68.9	28	14.57	22.57	28.56
	$H(z)$ + All BAO	0.34	-0.37	-0.64	-	65.7	37	35.06	43.06	50.01
	QSO	0.10	-0.55	-0.67	-	73.9	115	350.11	358.11	369.26
	QSO + $H(z)$ + BAO	0.32	-0.18	-0.73	-	65.5	157	387.67	395.67	408.02
Non-flat ϕ CDM	$H(z)$ only	0.36	-0.13	-	0.01	68.9	26	14.46	22.46	28.20
	$H(z)$ + 2 BAO	0.44	-0.48	-	0.51	69.2	28	14.54	22.54	28.53
	$H(z)$ + All BAO	0.32	-0.23	-	1.08	66.5	37	36.03	44.03	50.98
	QSO	0.10	-0.43	-	2.95	72.3	115	351	359	370.15
	QSO + $H(z)$ + BAO	0.32	-0.16	-	0.89	66.2	157	388.44	396.44	408.79

^a km s⁻¹Mpc⁻¹.

in this case). Park & Ratra (2018c) find $w_X = -0.72 \pm 0.16$ (-0.604 ± 0.099) for these two cases, from their $H(z)$ + BAO compilation, which favors quintessence-type dark energy over a Λ at 1.8σ (4σ). We find more significant evidence for dark energy dynamics in both the flat and non-flat ϕ CDM models, in which we measure $\alpha = 0.35^{+0.41+0.88}_{-0.21-0.32}$ and $\alpha = 1.19^{+0.48+0.94}_{-0.56-1.01}$, respectively (1σ and 2σ error bars). In both of these cases the measured values of α are a little more than 2σ away from $\alpha = 0$, which corresponds to Λ CDM. Our results for α are in less precise agreement with Park & Ratra (2018c) than the results for our other parameters. Park & Ratra (2018c) find for flat ϕ CDM $\alpha = 2.5 \pm 1.6$ at 1σ and $\alpha < 6.0$ at 2σ , while for non-flat ϕ CDM they find $\alpha = 3.1 \pm 1.5$ at 1σ .

Our results here cannot be directly compared to those of our earlier analyses (Ryan et al. 2018), since here H_0 is an adjustable parameter to be constrained by the data, while in Ryan et al. (2018) we marginalized over H_0 , assuming two different gaussian H_0 priors. However, we find that the results we have obtained, after marginalizing over H_0 with a flat prior, are qualitatively consistent with the results found in Ryan et al. (2018). Further, although we have compared our parameter measurements to those of Park & Ratra (2018c), a direct comparison of our best-fitting χ^2 values to the best-fitting χ^2 values of that paper is not possible because of the different numbers of parameters and data points those authors used,¹³ but we agree qualitatively with their result that there are only small differences between the χ^2 of the six models; for each data combination, the six models have relatively similar χ^2 , AIC, and BIC values (see Tables 3, 5, and 7).

5.2 QSO + $H(z)$ + BAO constraints

Our results for the full data set, consisting of QSO data combined with $H(z)$ and BAO data, are presented in Tables 3-8 and in Figs. A7-A12 below. As in Sec. 5.1 above, we have broken these results into three categories; here they are QSO

only (only the data points in Table 1 of Cao et al. 2017b), $H(z)$ + All BAO (identical to the $H(z)$ + All BAO category in Sec. 5.1) and QSO + $H(z)$ + BAO (the full data set). We retain the $H(z)$ + All BAO category here so that we can see the extent to which the addition of the QSO data tightens the constraints from $H(z)$ + All BAO alone, which we describe in detail below. By examining the two-dimensional constraint contours and one-dimensional likelihoods shown in Figs. A7-A12, we see that even though the QSO data by themselves are not able to tightly constrain cosmological parameters, they do contribute to a tightening of the constraints on these parameters when used in combination with $H(z)$ + All BAO data.¹⁴

As with the $H(z)$ + All BAO data combination, Ω_{m0} has consistent central value and error bars when it is measured with the full data set (see Tables 4, 6, and 8). For the flat and non-flat Λ CDM models, $\Omega_{m0} = 0.31^{+0.02}_{-0.01}$ and $\Omega_{m0} = 0.31^{+0.01}_{-0.01}$, respectively. For flat Λ CDM and flat ϕ CDM we find $\Omega_{m0} = 0.32^{+0.02}_{-0.01}$, while non-flat Λ CDM and non-flat ϕ CDM favor the slightly larger values $\Omega_{m0} = 0.32^{+0.02}_{-0.01}$ and $\Omega_{m0} = 0.32^{+0.01}_{-0.02}$, respectively. These measurements have very similar central values and error bars to the measurements made using the $H(z)$ + All BAO data combination, as shown by the one-dimensional likelihoods in Figs. A7-A12.

For flat (non-flat) Λ CDM we measure $H_0 = 68.18^{+0.70}_{-0.69}$ ($68.62^{+1.43}_{-1.44}$) km s⁻¹ Mpc⁻¹, while for flat (non-flat) Λ CDM $H_0 = 66.54^{+2.11}_{-1.82}$ ($65.3^{+2.0}_{-1.8}$) km s⁻¹ Mpc⁻¹, and for flat (non-flat) ϕ CDM we find $H_0 = 66.35^{+1.23}_{-1.69}$ ($65.8^{+1.8}_{-1.6}$) km s⁻¹ Mpc⁻¹, all 1σ error bars. Compared to the cases without the QSO data in Sec. 5.1, the central H_0 values here are a little larger (except in the non-flat Λ CDM and ϕ CDM cases) and the error bars are a little smaller. These H_0 estimates are still in very good agreement with that from median statistics (Chen & Ratra 2011a) but differ from that measured from the local expansion rate (Riess et al. 2018),

¹³ Park & Ratra (2018c) use a BAO measurement that we do not; instead of the one gaussian approximation constraint at $z = 2.36$ from Font-Ribera et al. (2014) in Table 1 here, Park & Ratra (2018c) use the probability distribution that describes the shift of the BAO peak position in both the perpendicular and parallel directions to the line of sight.

¹⁴ We confirm the high reduced χ^2 values for the QSO angular size data (see Tables 3, 5, and 7) found earlier by Zheng et al. (2017) (see Table 2 of that paper), Qi et al. (2017) (see Table 5 of that paper), and Xu et al. (2018) (see Table 2 of that paper). What causes this is apparently not yet understood.

Table 8. Best fitting parameters and 1σ and 2σ confidence intervals for the four-parameter models.

Model	Data set	Marginalization range ^a	Best-fitting	1σ	2σ
Non-flat Λ CDM	$H(z)$ only	$0.1 \leq \Omega_{m0} \leq 0.7$	$\Omega_{m0} = 0.25$	$0.16 \leq \Omega_{m0} \leq 0.41$	$0.11 \leq \Omega_{m0} \leq 0.54$
		$50 \leq H_0 \leq 85$	$H_0 = 66.2$	$62.1 \leq H_0 \leq 72.9$	$58.4 \leq H_0 \leq 79.6$
		$-2 \leq w_X \leq 0$	$w_X = -0.92$	$-1.59 \leq w_X \leq -0.57$	$-1.94 \leq w_X \leq -0.37$
		$-0.7 \leq \Omega_{k0} \leq 0.7$	$\Omega_{k0} = 0.18$	$-0.32 \leq \Omega_{k0} \leq 0.47$	$-0.63 \leq \Omega_{k0} \leq 0.65$
		$H(z) + 2$ BAO	$0.1 \leq \Omega_{m0} \leq 0.7$	$\Omega_{m0} = 0.41$	$0.31 \leq \Omega_{m0} \leq 0.51$
	$50 \leq H_0 \leq 85$	$H_0 = 69.2$	$65.5 \leq H_0 \leq 75.2$	$62.2 \leq H_0 \leq 81.4$	
	$-2 \leq w_X \leq 0$	$w_X = -0.88$	$-1.26 \leq w_X \leq -0.71$	$-1.68 \leq w_X \leq -0.59$	
	$-0.7 \leq \Omega_{k0} \leq 0.7$	$\Omega_{k0} = -0.34$	$-0.57 \leq \Omega_{k0} \leq -0.12$	$-0.68 \leq \Omega_{k0} \leq 0.06$	
	$H(z) +$ All BAO	$0.1 \leq \Omega_{m0} \leq 0.7$	$\Omega_{m0} = 0.33$	$0.31 \leq \Omega_{m0} \leq 0.35$	$0.29 \leq \Omega_{m0} \leq 0.37$
	$50 \leq H_0 \leq 85$	$H_0 = 65.5$	$63.3 \leq H_0 \leq 67.9$	$61.2 \leq H_0 \leq 70.3$	
	$-2 \leq w_X \leq 0$	$w_X = -0.63$	$-0.78 \leq w_X \leq -0.58$	$-0.98 \leq w_X \leq -0.54$	
	$-0.7 \leq \Omega_{k0} \leq 0.7$	$\Omega_{k0} = -0.24$	$-0.5 \leq \Omega_{k0} \leq -0.06$	$-0.6 \leq \Omega_{k0} \leq 0.10$	
	QSO	$0.1 \leq \Omega_{m0} \leq 0.7$	$\Omega_{m0} = 0.29$	$0.19 \leq \Omega_{m0} \leq 0.48$	$0.12 \leq \Omega_{m0} \leq 0.65$
	$50 \leq H_0 \leq 85$	$H_0 = 60.5$	$57.2 \leq H_0 \leq 71.3$	$54.3 \leq H_0 \leq 81.3$	
	$-2 \leq w_X \leq 0$	$w_X = -0.74$	$-1.51 \leq w_X \leq -0.36$	$-1.92 \leq w_X \leq -0.07$	
	$-0.7 \leq \Omega_{k0} \leq 0.7$	$\Omega_{k0} = 0.04$	$-0.29 \leq \Omega_{k0} \leq 0.48$	$-0.54 \leq \Omega_{k0} \leq 0.67$	
	QSO + $H(z)$ + BAO	$0.1 \leq \Omega_{m0} \leq 0.7$	$\Omega_{m0} = 0.32$	$0.31 \leq \Omega_{m0} \leq 0.34$	$0.29 \leq \Omega_{m0} \leq 0.35$
	$50 \leq H_0 \leq 85$	$H_0 = 65.3$	$63.5 \leq H_0 \leq 67.3$	$61.9 \leq H_0 \leq 69.5$	
	$-2 \leq w_X \leq 0$	$w_X = -0.71$	$-0.84 \leq w_X \leq -0.64$	$-1.01 \leq w_X \leq -0.57$	
	$-0.7 \leq \Omega_{k0} \leq 0.7$	$\Omega_{k0} = -0.15$	$-0.28 \leq \Omega_{k0} \leq -0.05$	$-0.40 \leq \Omega_{k0} \leq 0.05$	
Non-flat ϕ CDM	$H(z)$ only	$0.1 \leq \Omega_{m0} \leq 0.7$	$\Omega_{m0} = 0.22$	$0.15 \leq \Omega_{m0} \leq 0.35$	$0.11 \leq \Omega_{m0} \leq 0.47$
		$50 \leq H_0 \leq 85$	$H_0 = 64.3$	$61.3 \leq H_0 \leq 67.9$	$58.3 \leq H_0 \leq 71.7$
		N/A	N/A	N/A	N/A
		N/A	N/A	N/A	N/A
		$H(z) + 2$ BAO	$0.1 \leq \Omega_{m0} \leq 0.7$	$\Omega_{m0} = 0.37$	$0.29 \leq \Omega_{m0} \leq 0.44$
	$50 \leq H_0 \leq 85$	$H_0 = 68.2$	$65.1 \leq H_0 \leq 71.3$	$61.9 \leq H_0 \leq 74.3$	
	$0.01 \leq \alpha \leq 5$	$\alpha = 0.20$	$0.01 \leq \alpha \leq 0.99$	$0.01 \leq \alpha \leq 1.74$	
	$-0.5 \leq \Omega_{k0} \leq 0.5$	$\Omega_{k0} = -0.5$	$\Omega_{k0} \leq -0.25$	$\Omega_{k0} \leq -0.04$	
	$H(z) +$ All BAO	$0.1 \leq \Omega_{m0} \leq 0.7$	$\Omega_{m0} = 0.32$	$0.30 \leq \Omega_{m0} \leq 0.34$	$0.29 \leq \Omega_{m0} \leq 0.35$
	$50 \leq H_0 \leq 85$	$H_0 = 66.0$	$63.8 \leq H_0 \leq 68.4$	$61.6 \leq H_0 \leq 70.7$	
	$0.01 \leq \alpha \leq 5$	$\alpha = 1.19$	$0.63 \leq \alpha \leq 1.67$	$0.18 \leq \alpha \leq 2.13$	
	$-0.5 \leq \Omega_{k0} \leq 0.5$	$\Omega_{k0} = -0.23$	$-0.38 \leq \Omega_{k0} \leq -0.07$	$-0.48 \leq \Omega_{k0} \leq 0.06$	
	QSO	$0.1 \leq \Omega_{m0} \leq 0.7$	$\Omega_{m0} = 0.21$	$0.14 \leq \Omega_{m0} \leq 0.42$	$0.11 \leq \Omega_{m0} \leq 0.62$
	$50 \leq H_0 \leq 85$	$H_0 = 62.5$	$58.4 \leq H_0 \leq 69.0$	$55.6 \leq H_0 \leq 76.4$	
	N/A	N/A	N/A	N/A	
	N/A	N/A	N/A	N/A	
	QSO + $H(z)$ + All BAO	$0.1 \leq \Omega_{m0} \leq 0.7$	$\Omega_{m0} = 0.32$	$0.30 \leq \Omega_{m0} \leq 0.33$	$0.29 \leq \Omega_{m0} \leq 0.35$
	$50 \leq H_0 \leq 85$	$H_0 = 65.8$	$64.2 \leq H_0 \leq 67.6$	$62.6 \leq H_0 \leq 69.3$	
	$0.01 \leq \alpha \leq 5$	$\alpha = 0.92$	$0.48 \leq \alpha \leq 1.46$	$0.13 \leq \alpha \leq 1.97$	
	$-0.5 \leq \Omega_{k0} \leq 0.5$	$\Omega_{k0} = -0.17$	$-0.28 \leq \Omega_{k0} \leq -0.07$	$-0.40 \leq \Omega_{k0} \leq 0.02$	

^a H_0 has units of $\text{km s}^{-1}\text{Mpc}^{-1}$.

being between 2.2σ (non-flat Λ CDM) and 3.5σ (flat ϕ CDM) lower.

When we measure the curvature energy density parameter using the full data set, we find in the non-flat Λ CDM model that $\Omega_{k0} = -0.01^{+0.05}_{-0.06}$, which is again consistent with flat spatial hypersurfaces, but with tighter error bars. The same pattern holds when we measure Ω_{k0} in the non-flat XCDM parametrization and the non-flat ϕ CDM model, in which $\Omega_{k0} = -0.15^{+0.10}_{-0.13}$ and $\Omega_{k0} = -0.17^{+0.10}_{-0.11}$, respectively. Both of these measurements are again consistent with closed spatial hypersurfaces, but they are 1.5σ (non-flat XCDM) and 1.7σ (non-flat ϕ CDM) away from spatial flatness.

The parameters that govern dark energy dynamics move

closer to Λ CDM when we measure them with the full data set. In the flat (non-flat) XCDM parametrization, $w_X = -0.91^{+0.09}_{-0.11}$ ($w_X = -0.71^{+0.07}_{-0.13}$), with 1σ error bars. In both cases we find that the addition of QSO data to the $H(z)$ + All BAO data drives the value of w_X closer to $w_X = -1$, the value that it takes in the flat and non-flat Λ CDM models (although w_X is still about 1σ larger than -1). Something similar happens to α ; in the flat (non-flat) ϕ CDM model we measure $\alpha = 0.21^{+0.35+0.73}_{-0.13-0.19}$ ($\alpha = 0.92^{+0.54+1.05}_{-0.44-0.79}$), with 1 and 2σ error bars that are tighter than they are when α is measured using only $H(z)$ + All BAO data. As in XCDM, the parameter that controls the dark energy dynamics, α , is driven

closer to $\alpha = 0$, the value that it takes when ϕ CDM reduces to Λ CDM (though α is still measured to be about 2σ away from zero).

6 CONCLUSION

We analyzed a total of 162 observations, 120 of which were measurements of the QSO angular sizes from Cao et al. (2017b), with the remaining 42 measurements being a combination of $H(z)$ data and distance measurements from baryon acoustic oscillations (compiled in Ryan et al. 2018).

Our methods and models were largely the same in this paper as in Ryan et al. (2018), with a few key differences. First, we treated H_0 as a free parameter, so as to obtain constraints on its value within the models we studied. We also presented results for each of our data sets separately and in combination (in Ryan et al. 2018 we only presented results for the $H(z)$ + BAO data combination), and treated the sound horizon and D_M - $H(z)$ covariance matrix more accurately (see Sec. 4).

We find that adding QSO data to $H(z)$ and BAO data tightens parameter constraints in the models we studied, and that the QSO data have a fairly large reduced $\chi^2 \sim 3$, the causes of which are apparently not yet understood.

Our results for the energy density parameters Ω_{m0} and Ω_Λ , the dark energy equation of state w_X , and the ϕ CDM potential energy density parameter α for the $H(z)$ + BAO combination are largely consistent with the results of Ryan et al. (2018), after accounting for slight differences due to the changes in our methods from that paper. In particular, we find that there is some evidence for closed spatial hypersurfaces in dynamical dark energy models, but that this evidence is only marginally significant at 1.3 or 1.4σ . We also find that there is evidence for dark energy dynamics in both flat and non-flat models, ranging from a little more than 1σ to a little more than 2σ . A little more significant is the evidence we find in favor of a lower value of the Hubble constant. Our H_0 results are more consistent with the results of Chen & Ratra (2011a) and Planck Collaboration (2018) than that of Riess et al. (2018), being between 2.2σ and 3.5σ lower, depending on the model considered.

ACKNOWLEDGEMENTS

We thank Chan-Gyung Park and Lado Samushia for helpful discussions, and we thank Dave Turner for providing valuable technical advice. Some of the computing for this project was performed on the Beocat Research Cluster at Kansas State University, which is funded in part by NSF grants CNS-1006860, EPS-1006860, and EPS-0919443. This work was partially funded by DOE Grant DE-SC0019038. YC received support from the National Natural Science Foundation of China (Nos. 11703034, 11773032 and 11573031), and the NAOC Nebula Talents Program.

REFERENCES

Alam S., et al., 2017, *MNRAS*, **470**, 2617
Anagnostopoulos F. K., Basilakos S., 2018, *Phys. Rev. D*, **97**, 063503

Ata M., et al., 2018, *MNRAS*, **473**, 4773
Avsajanishvili O., Samushia L., Arhipova N. A., Kahniashvili T., 2015, preprint, ([arXiv:1511.09317](https://arxiv.org/abs/1511.09317))
Bautista J. E., et al., 2017, *A&A*, **603**, A12
Beutler F., et al., 2011, *MNRAS*, **416**, 3017
Bonamente M., Joy M. K., LaRoque S. J., Carlstrom J. E., Reese E. D., Dawson K. S., 2006, *ApJ*, **647**, 25
Cao S., Biesiada M., Jackson J., Zheng X., Zhao Y., Zhu Z.-H., 2017a, *J. Cosmology Astropart. Phys.*, **2**, 012
Cao S., Zheng X., Biesiada M., Qi J., Chen Y., Zhu Z.-H., 2017b, *A&A*, **606**, A15
Chen G., Ratra B., 2003, *ApJ*, **582**, 586
Chen G., Ratra B., 2011a, *PASP*, **123**, 1127
Chen Y., Ratra B., 2011b, *Physics Letters B*, **703**, 406
Chen Y., Ratra B., 2012, *A&A*, **543**, A104
Chen G., Gott III J. R., Ratra B., 2003, *PASP*, **115**, 1269
Chen Y., Geng C.-Q., Cao S., Huang Y.-M., Zhu Z.-H., 2015, *J. Cosmology Astropart. Phys.*, **2**, 010
Chen Y., Ratra B., Biesiada M., Li S., Zhu Z.-H., 2016, *ApJ*, **829**, 61
Chen Y., Kumar S., Ratra B., 2017, *ApJ*, **835**, 86
DES Collaboration 2018a, preprint, ([arXiv:1810.02499](https://arxiv.org/abs/1810.02499))
DES Collaboration 2018b, *MNRAS*, **480**, 3879
da Silva G. P., Cavalcanti A. G., 2018, *Brazilian Journal of Physics*, **48**, 521
Daly R. A., Guerra E. J., 2002, *AJ*, **124**, 1831
Dhawan S., Jha S. W., Leibundgut B., 2018, *A&A*, **609**, A72
Eisenstein D. J., Hu W., 1998, *ApJ*, **496**, 605
Farooq O., 2013, PhD thesis, Kansas State U. ([arXiv:1309.3710](https://arxiv.org/abs/1309.3710))
Farooq O., Ratra B., 2013, *ApJ*, **766**, L7
Farooq O., Crandall S., Ratra B., 2013, *Physics Letters B*, **726**, 72
Farooq O., Mania D., Ratra B., 2015, *Ap&SS*, **357**, 11
Farooq O., Ranjeet Madiyar F., Crandall S., Ratra B., 2017, *ApJ*, **835**, 26
Fernández Arenas D., et al., 2018, *MNRAS*, **474**, 1250
Font-Ribera A., et al., 2014, *J. Cosmology Astropart. Phys.*, **5**, 027
Geng J.-J., Guo R.-Y., Wang A.-Z., Zhang J.-F., Zhang X., 2018, *Communications in Theoretical Physics*, **70**, 445
Gómez-Valent A., 2018, preprint, ([arXiv:1810.02278](https://arxiv.org/abs/1810.02278))
Gómez-Valent A., Amendola L., 2018, *J. Cosmology Astropart. Phys.*, **4**, 051
Gott III J. R., 1982, *Nature*, **295**, 304
Gott III J. R., Vogeley M. S., Podariu S., Ratra B., 2001, *ApJ*, **549**, 1
Gurvits L. I., Kellermann K. I., Frey S., 1999, *A&A*, **342**, 378
Hawking S. W., 1984, *Nuclear Physics B*, **239**, 257
Hogg D. W., 1999, preprint, ([arXiv:astro-ph/9905116](https://arxiv.org/abs/astro-ph/9905116))
Jesus J. F., Holanda R. F. L., Pereira S. H., 2018, *J. Cosmology Astropart. Phys.*, **5**, 073
Li X., Cao S., Zheng X., Qi J., Biesiada M., Zhu Z.-H., 2017, preprint, ([arXiv:1708.08867](https://arxiv.org/abs/1708.08867))
Liddle A. R., 2007, *MNRAS*, **377**, L74
Lima J. A. S., Alcaniz J. S., 2002, *ApJ*, **566**, 15
Lin W., Ishak M., 2017, *Phys. Rev. D*, **96**, 083532
Liu Y., Guo R.-Y., Zhang J.-F., Zhang X., 2018, preprint, ([arXiv:1811.12131](https://arxiv.org/abs/1811.12131))
Mamon A. A., Bamba K., 2018, preprint, ([arXiv:1805.02854](https://arxiv.org/abs/1805.02854))
Mitra S., Choudhury T. R., Ratra B., 2018, *MNRAS*, **479**, 4566
Mitra S., Park C.-G., Choudhury T. R., Ratra B., 2019, preprint, ([arXiv:1901.09927](https://arxiv.org/abs/1901.09927))
Moresco M., et al., 2016a, *J. Cosmology Astropart. Phys.*, **5**, 014
Moresco M., Jimenez R., Verde L., Cimatti A., Pozzetti L., Maraston C., Thomas D., 2016b, *J. Cosmology Astropart. Phys.*, **12**, 039
Mukherjee A., Paul N., Jassal H. K., 2019, *J. Cosmology Astropart. Phys.*, **1**, 005

Ooba J., Ratra B., Sugiyama N., 2018a, preprint, ([arXiv:1802.05571](#))

Ooba J., Ratra B., Sugiyama N., 2018b, *ApJ*, **864**, 80

Ooba J., Ratra B., Sugiyama N., 2018c, *ApJ*, **866**, 68

Ooba J., Ratra B., Sugiyama N., 2018d, *ApJ*, **869**, 34

Park C.-G., Ratra B., 2018a, preprint, ([arXiv:1801.00213](#))

Park C.-G., Ratra B., 2018b, preprint, ([arXiv:1803.05522](#))

Park C.-G., Ratra B., 2018c, preprint, ([arXiv:1809.03598](#))

Park C.-G., Ratra B., 2018d, *ApJ*, **868**, 83

Pavlov A., Westmoreland S., Saaidi K., Ratra B., 2013, *Phys. Rev. D*, **88**, 123513

Peebles P. J. E., 1984, *ApJ*, **284**, 439

Peebles P. J. E., Ratra B., 1988, *ApJ*, **325**, L17

Penton J., Peyton J., Zahoor A., Ratra B., 2018, *PASP*, **130**, 114001

Planck Collaboration 2016, *A&A*, **594**, A13

Planck Collaboration 2018, preprint, ([arXiv:1807.06209](#))

Podariu S., Daly R. A., Mory M. P., Ratra B., 2003, *ApJ*, **584**, 577

Qi J.-Z., Cao S., Biesiada M., Zheng X., Zhu Z.-H., 2017, *European Physical Journal C*, **77**, 502

Qi J.-Z., Cao S., Zhang S., Biesiada M., Wu Y., Zhu Z.-H., 2018, preprint, ([arXiv:1803.01990](#))

Rana A., Jain D., Mahajan S., Mukherjee A., 2017, *J. Cosmology Astropart. Phys.*, **3**, 028

Ratra B., 1985, *Phys. Rev. D*, **31**, 1931

Ratra B., 2017, *Phys. Rev. D*, **96**, 103534

Ratra B., Peebles P. J. E., 1988, *Phys. Rev. D*, **37**, 3406

Ratra B., Peebles P. J. E., 1995, *Phys. Rev. D*, **52**, 1837

Riess A. G., et al., 2016, *ApJ*, **826**, 56

Riess A. G., et al., 2018, *ApJ*, **855**, 136

Ross A. J., Samushia L., Howlett C., Percival W. J., Burden A., Manera M., 2015, *MNRAS*, **449**, 835

Ruan C.-Z., Fulvio M., Yu C., Tong-Jie Z., 2019, preprint, ([arXiv:1901.06626](#))

Ryan J., Doshi S., Ratra B., 2018, *MNRAS*, **480**, 759

Samushia L., Ratra B., 2010, *ApJ*, **714**, 1347

Samushia L., Chen G., Ratra B., 2007, preprint, ([arXiv:0706.1963](#))

Samushia L., Dev A., Jain D., Ratra B., 2010, *Physics Letters B*, **693**, 509

Sangwan A., Tripathi A., Jassal H. K., 2018, preprint, ([arXiv:1804.09350](#))

Scolnic D. M., et al., 2018, *ApJ*, **859**, 101

Singh A., Sangwan A., Jassal H. K., 2018, preprint, ([arXiv:1811.07513](#))

Sola J., Gomez-Valent A., de Cruz Perez J., 2018, preprint, ([arXiv:1811.03505](#))

Tosone F., Haridasu B. S., Luković V. V., Vittorio N., 2018, preprint, ([arXiv:1811.05434](#))

Vishwakarma R. G., 2001, *Classical and Quantum Gravity*, **18**, 1159

Wang Y., Xu L., Zhao G.-B., 2017, *ApJ*, **849**, 84

Wang Y., Pogosian L., Zhao G.-B., Zucca A., 2018, *ApJ*, **869**, L8

Wei J.-J., 2018, *ApJ*, **868**, 29

Wei J.-J., Wu X.-F., 2017, *ApJ*, **838**, 160

Witzemann A., Bull P., Clarkson C., Santos M. G., Spinelli M., Weltman A., 2018, *MNRAS*, **477**, L122

Xu T., Cao S., Qi J., Biesiada M., Zheng X., Zhu Z.-H., 2018, *J. Cosmology Astropart. Phys.*, **6**, 042

Yang W., Shahalam M., Pal B., Pan S., Wang A., 2018, preprint, ([arXiv:1810.08586](#))

Yashar M., Bozek B., Abrahamse A., Albrecht A., Barnard M., 2009, *Phys. Rev. D*, **79**, 103004

Yu H., Wang F. Y., 2016, *ApJ*, **828**, 85

Yu H., Ratra B., Wang F.-Y., 2018, *ApJ*, **856**, 3

Zhai Z., Blanton M., Slosar A., Tinker J., 2017, *ApJ*, **850**, 183

Zhang J., 2018, *PASP*, **130**, 084502

Zhang X., Huang Q.-G., 2018, preprint, ([arXiv:1812.01877](#))

Zhang Y.-C., Zhang H.-Y., Wang D.-D., Qi Y.-H., Wang Y.-T., Zhao G.-B., 2017a, *Research in Astronomy and Astrophysics*, **17**, 050

Zhang B. R., Childress M. J., Davis T. M., Karpenka N. V., Lidman C., Schmidt B. P., Smith M., 2017b, *MNRAS*, **471**, 2254

Zhang J.-J., Lee C.-C., Geng C.-Q., 2018, preprint, ([arXiv:1812.06710](#))

Zhang X., Huang Q.-G., Li X.-D., 2019, *MNRAS*, **483**, 1655

Zheng X., Biesiada M., Cao S., Qi J., Zhu Z.-H., 2017, *J. Cosmology Astropart. Phys.*, **10**, 030

Zheng J., Melia F., Zhang T.-J., 2019, preprint, ([arXiv:1901.05705](#))

Zhu Z.-H., Fujimoto M.-K., 2002, *ApJ*, **581**, 1

APPENDIX A: PLOTS OF 2D AND 1D CONSTRAINTS ON MODEL PARAMETERS FROM QSO, $H(z)$, AND BAO DATA

In all two-dimensional confidence contour plots, the 1, 2, and 3σ confidence contours demarcate regions of the two-dimensional parameter space separated by intervals of $\chi^2_{\min} + 2.3$, $\chi^2_{\min} + 6.17$, and $\chi^2_{\min} + 11.8$, respectively. In the two-dimensional confidence contour plots and one-dimensional likelihood plots of Figs. A1-A6, dotted black lines represent the constraints from $H(z)$ data, dashed black lines represent the constraints from $H(z) + 2$ BAO data, and solid black lines represent the constraints from $H(z) +$ BAO data. In the two-dimensional confidence contour plots, the location of χ^2_{\min} in the parameter space is indicated by a green "x" for the $H(z)$ data, a blue "+" for the $H(z) + 2$ BAO data, and a red dot for the $H(z) +$ All BAO data.

In the two-dimensional confidence contour plots and one-dimensional likelihood plots of Figs. A7-A12, dotted black lines represent the constraints from QSO data, dashed black lines represent the constraints from $H(z) +$ All BAO data, and solid black lines represent the constraints from QSO + $H(z) +$ BAO data. In the two-dimensional confidence contour plots, a green "x" indicates the location of χ^2_{\min} for the QSO data, a blue "+" indicates the location of χ^2_{\min} for the $H(z) +$ BAO data, and a red dot indicates the location of χ^2_{\min} for the QSO + $H(z) +$ BAO data.

This paper has been typeset from a $\text{\TeX}/\text{\LaTeX}$ file prepared by the author.

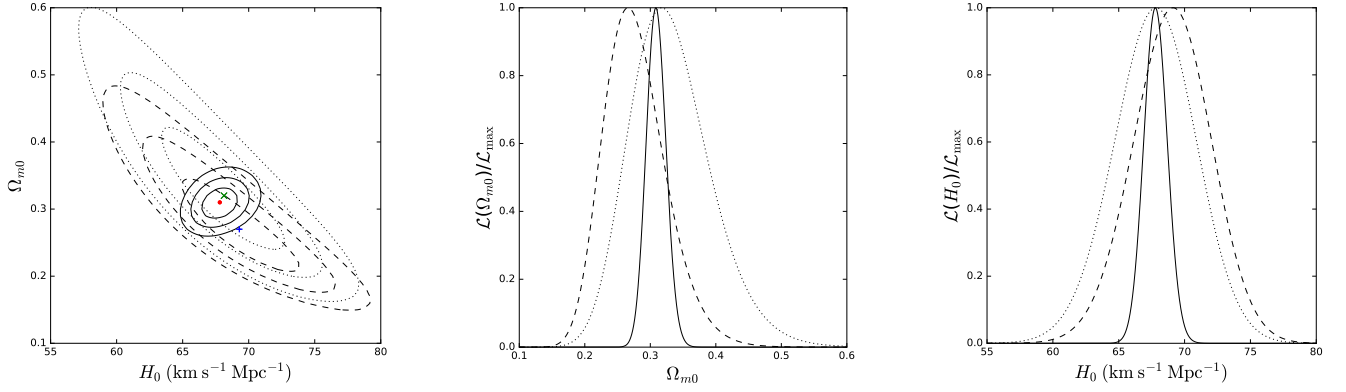


Figure A1. Flat Λ CDM model with $H(z)$ and BAO data. Left panel: 1, 2, and 3σ confidence contours and best-fitting points. Center and right panels: One-dimensional likelihoods for Ω_{m0} and H_0 . See text for description and discussion.

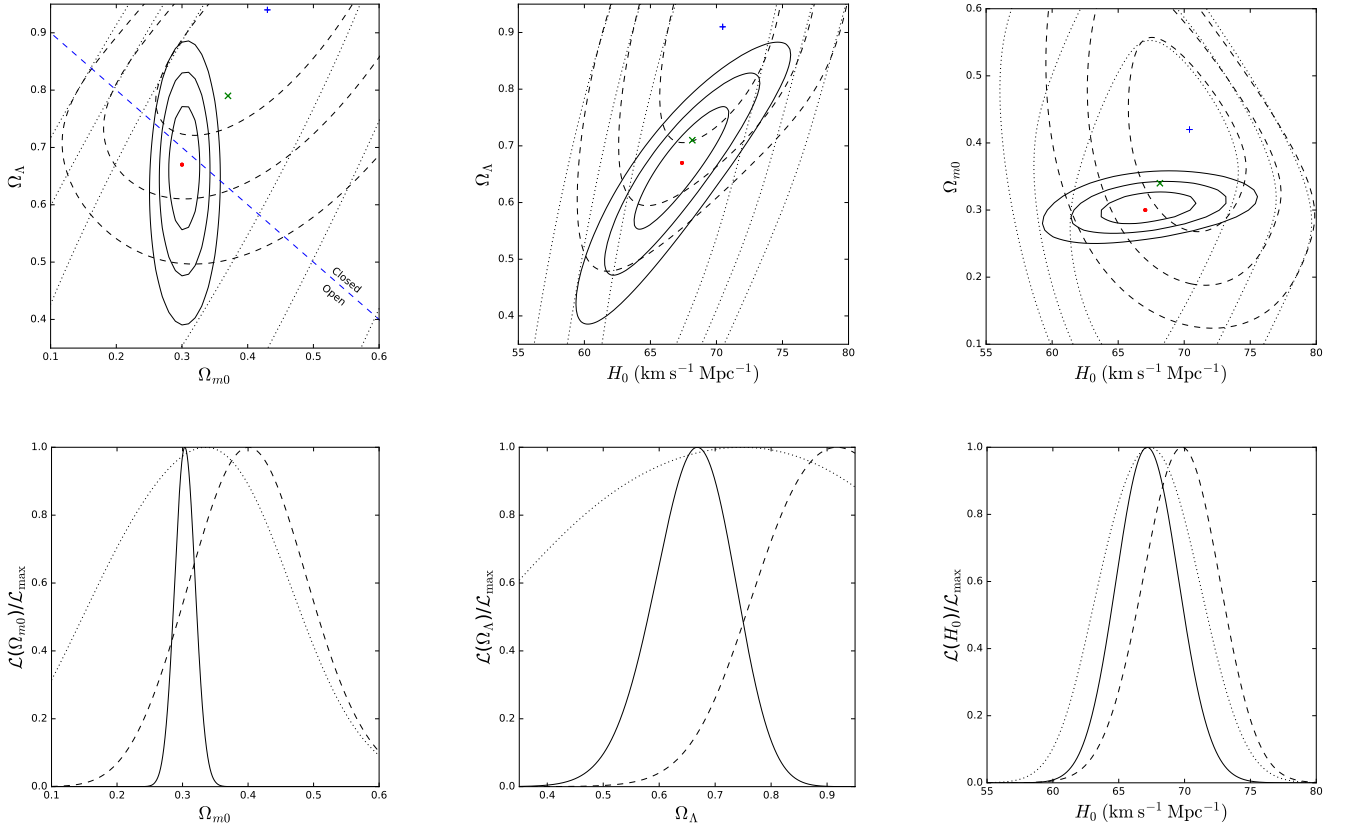


Figure A2. Non-flat Λ CDM model with $H(z)$ and BAO data. Top panels: 1, 2, and 3σ confidence contours and best-fitting points. In the top left panel, the blue dashed line demarcates regions of the Ω_{m0} - Ω_Λ parameter space that correspond to spatially open and spatially closed models. Points on the line correspond to the spatially flat model. Bottom panels: one-dimensional likelihoods for Ω_{m0} , Ω_Λ , and H_0 . See text for description and discussion.

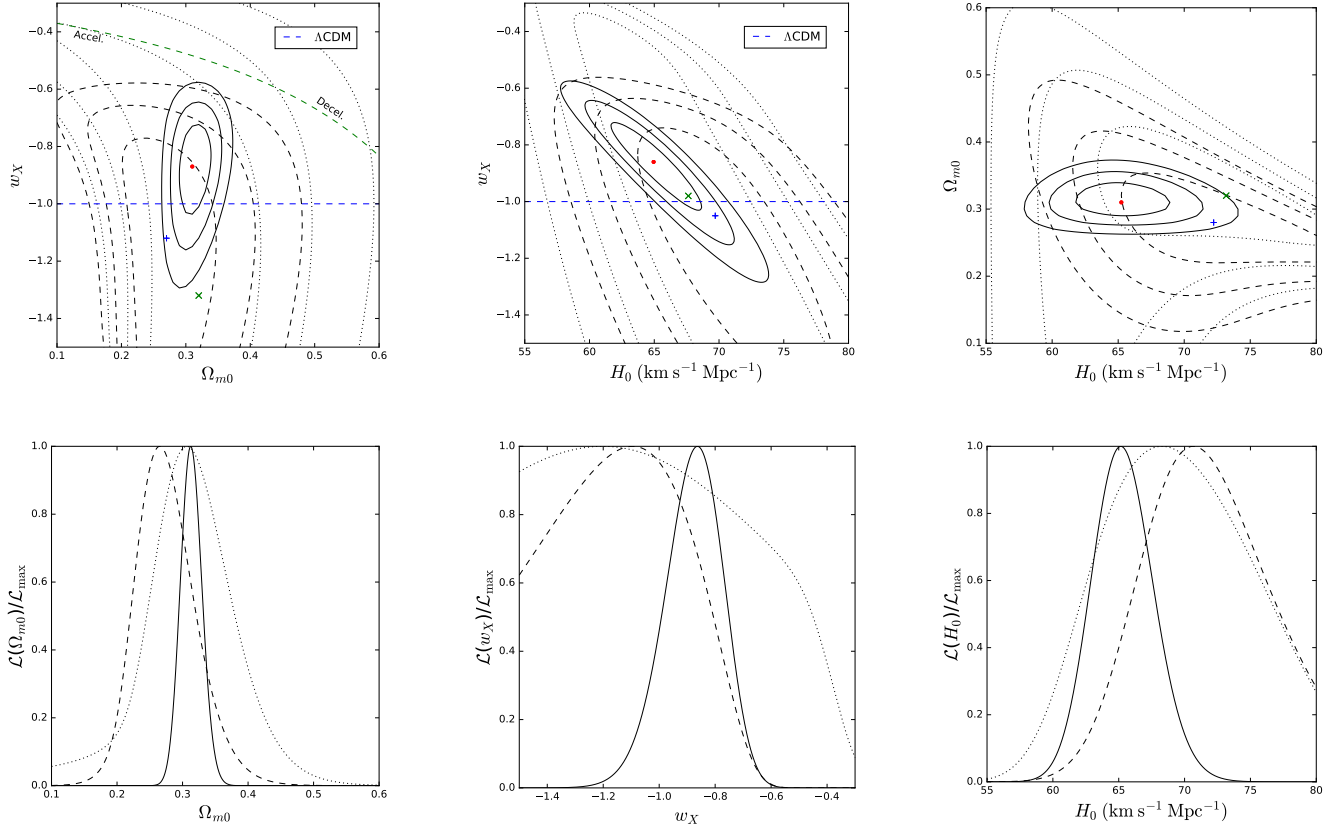


Figure A3. Flat XCDM parametrization with $H(z)$ and BAO data. Top panels: 1, 2, and 3σ confidence contours and best-fitting points. In the top left and top center panels the horizontal blue dashed line separates quintessence-type parametrizations of dark energy (for which $w_X > -1$) from phantom-type parametrizations of dark energy (for which $w_X < -1$). Points on the blue line (for which $w_X = -1$) correspond to the flat Λ CDM model. The green dashed curve in the left panel separates models that undergo accelerated expansion now from models that undergo decelerated expansion now. Bottom panels: one-dimensional likelihoods for Ω_{m0} , w_X , and H_0 . See text for description and discussion.

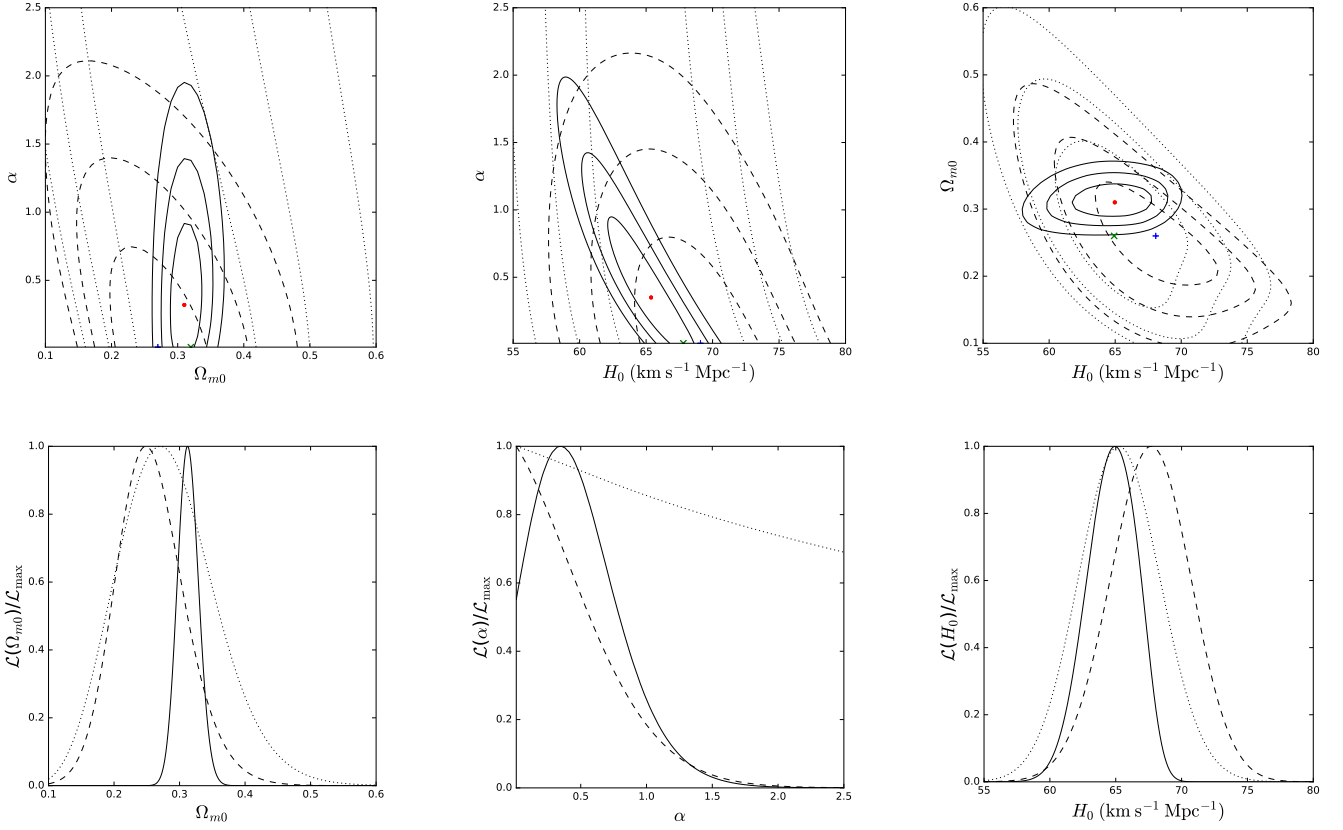


Figure A4. Flat ϕ CDM model with $H(z)$ and BAO data. Top panels: 1, 2, and 3σ confidence contours and best-fitting points. Points on the $\alpha = 0$ line in the top left and top center panels correspond to the flat Λ CDM model. Bottom panels: one-dimensional likelihoods of Ω_{m0} , α , and H_0 . See text for description and discussion.

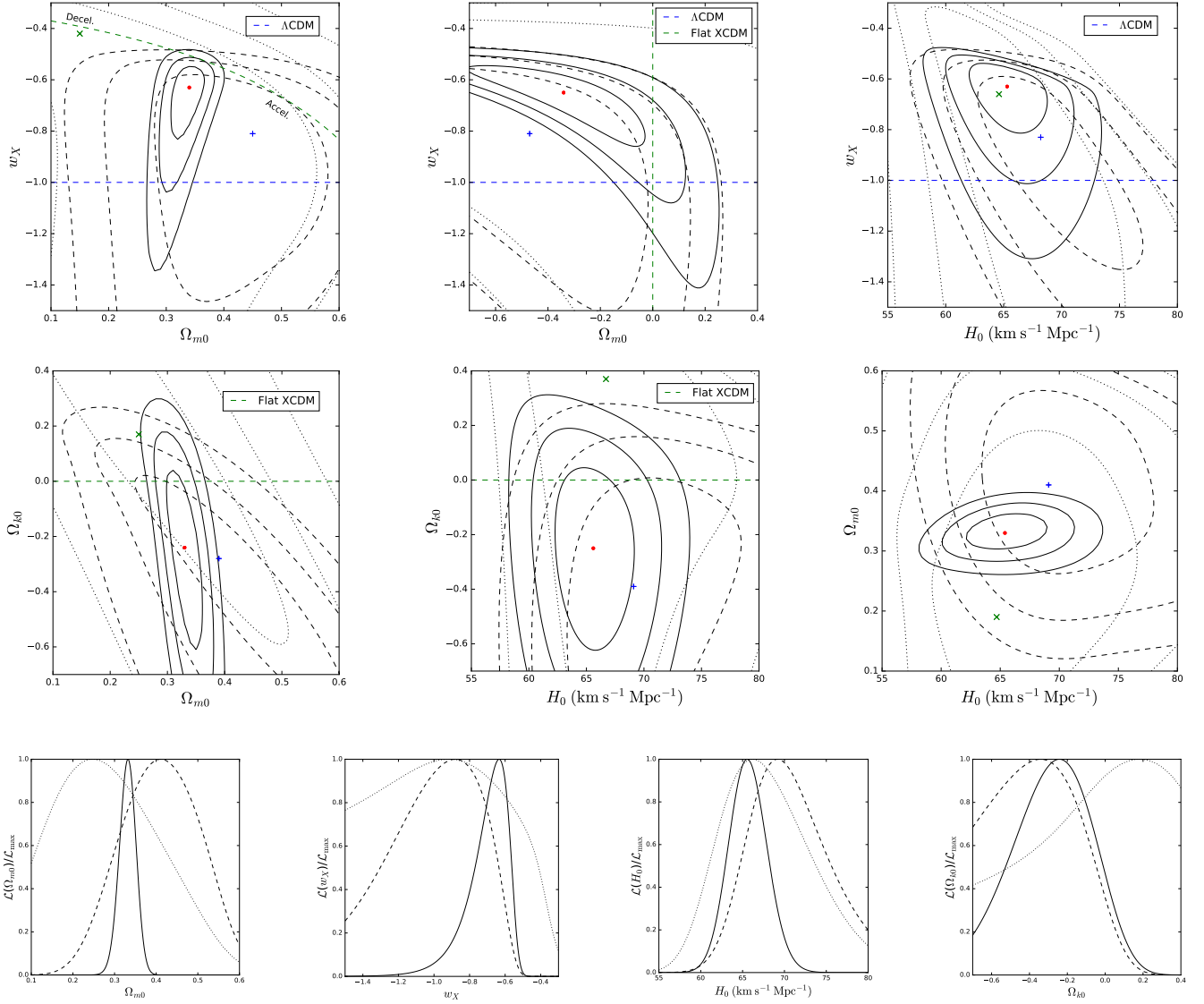


Figure A5. Non-flat XCDM parametrization with $H(z)$ and BAO data. Top and middle row: 1, 2, and 3σ confidence contours and best-fitting points. In the top panels, the horizontal blue dashed line separates quintessence-type parametrizations of dark energy (for which $w_X > -1$) from phantom-type parametrization of dark energy (for which $w_X < -1$). Points on the blue line (for which $w_X = -1$) correspond to the non-flat Λ CDM model. The green dashed curve in the top left panel separates models that undergo accelerated expansion now from models that undergo decelerated expansion now. The vertical green dashed line in the top center panel, and the horizontal green dashed lines in the left and center panels of the middle row, separate spatially closed models (for which $\Omega_{k0} < 0$) from spatially open models (for which $\Omega_{k0} > 0$). Bottom panels: one-dimensional likelihoods for Ω_{m0} , w_X , H_0 , and Ω_{k0} . See text for description and discussion.

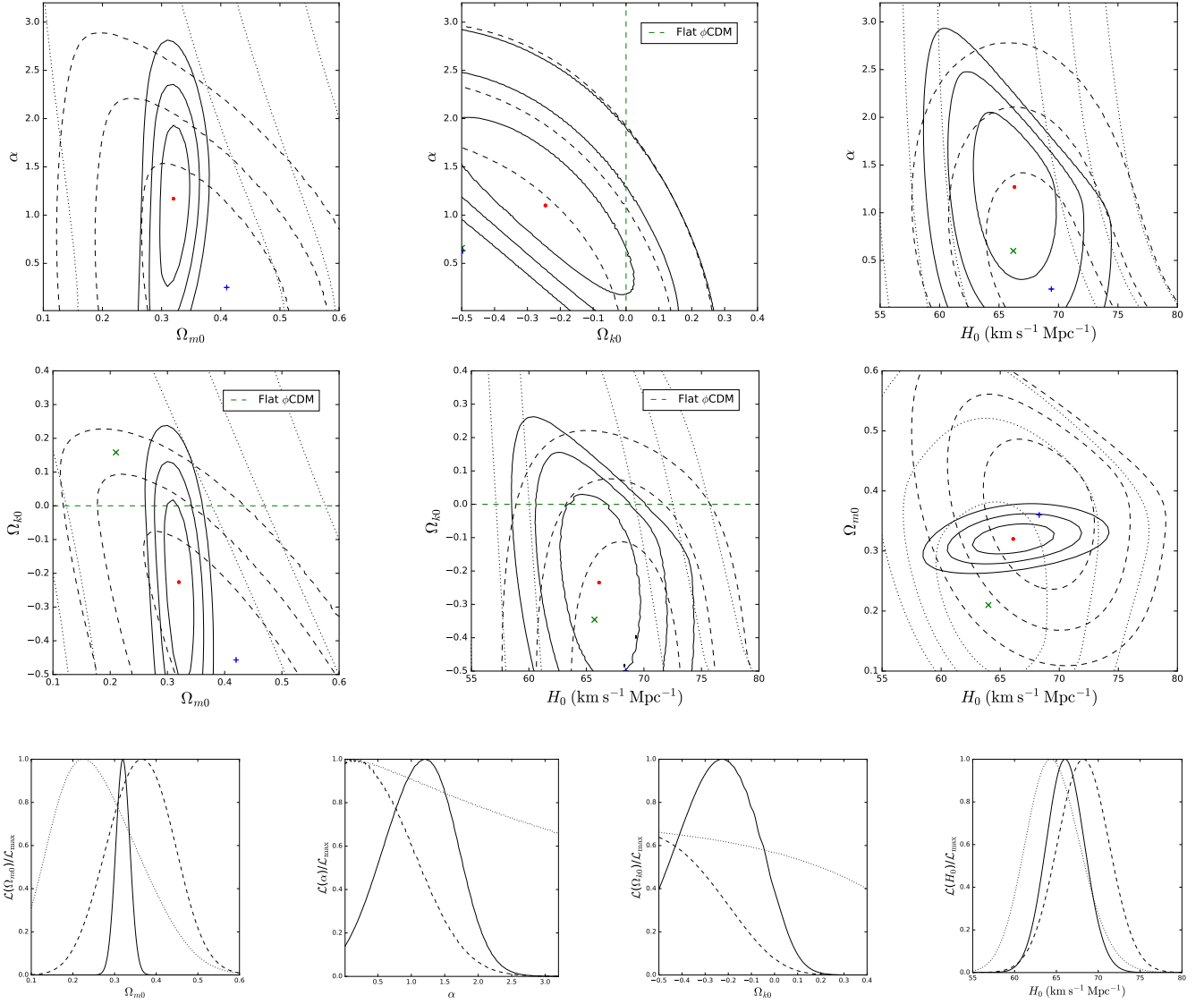


Figure A6. Non-flat ϕ CDM model with $H(z)$ and BAO data. Top and middle rows: 1, 2, and 3 σ confidence contours and best-fitting points. The vertical green dashed line in the top center panel, and the horizontal green dashed lines in the middle left and middle center panels, separate spatially closed models (with $\Omega_{k0} < 0$) from spatially open models (with $\Omega_{k0} > 0$). Points on the $\alpha = 0$ line in the top panels correspond to the non-flat Λ CDM model. Bottom row: one-dimensional likelihoods for Ω_{m0} , α , Ω_{k0} , and H_0 . See text for description and discussion.

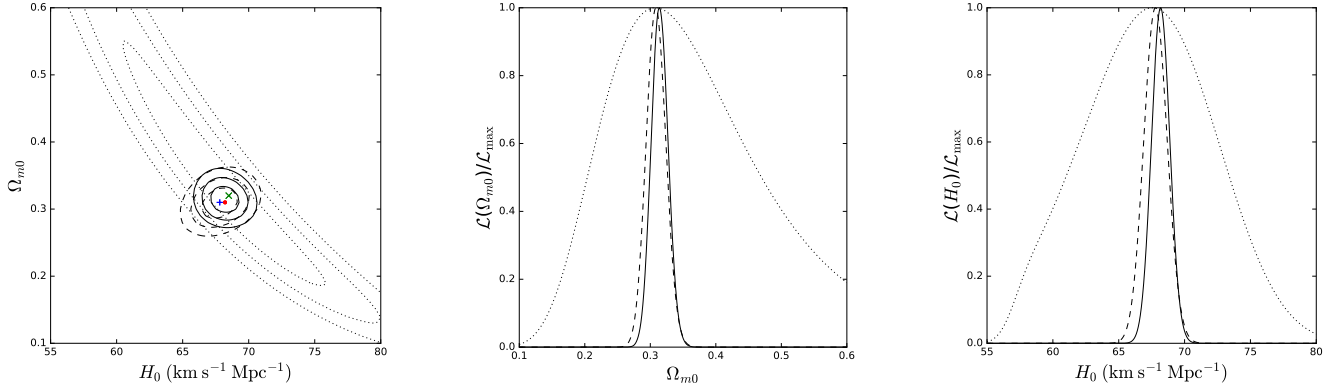


Figure A7. Flat Λ CDM model with QSO, $H(z)$, and BAO data. Left panel: 1, 2, and 3σ confidence contours and best-fitting points. Center and right panels: one-dimensional likelihoods for Ω_{m0} and H_0 . See text for description and discussion.

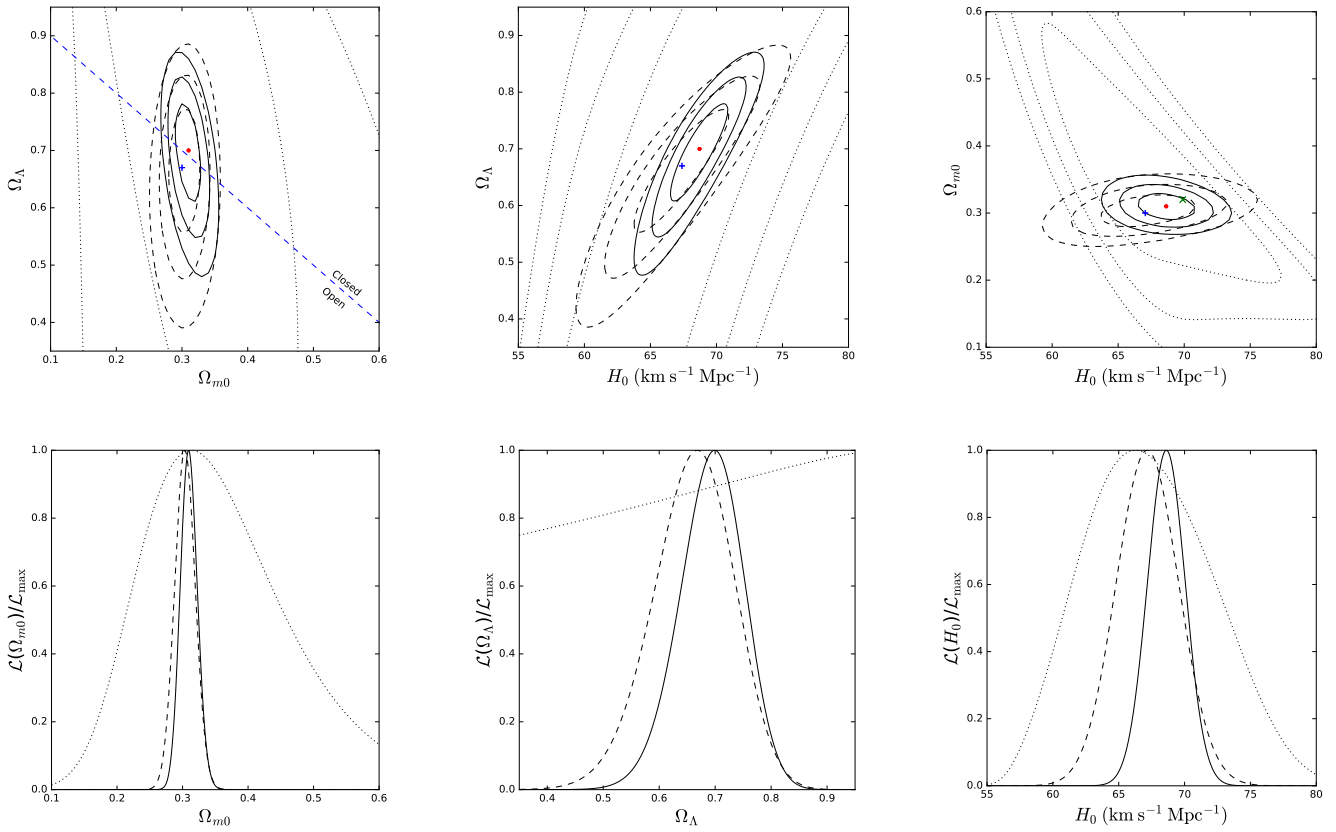


Figure A8. Non-flat Λ CDM model with QSO, $H(z)$, and BAO data. In the top left panel, the blue dashed line demarcates regions of the Ω_{m0} - Ω_Λ parameter space that correspond to spatially open ($\Omega_{k0} > 0$) and spatially closed ($\Omega_{k0} < 0$) models. Points on the line correspond to spatially flat models, with $\Omega_{k0} = 0$. Bottom panels: one-dimensional likelihoods for Ω_{m0} , Ω_Λ , and H_0 . See text for description and discussion.

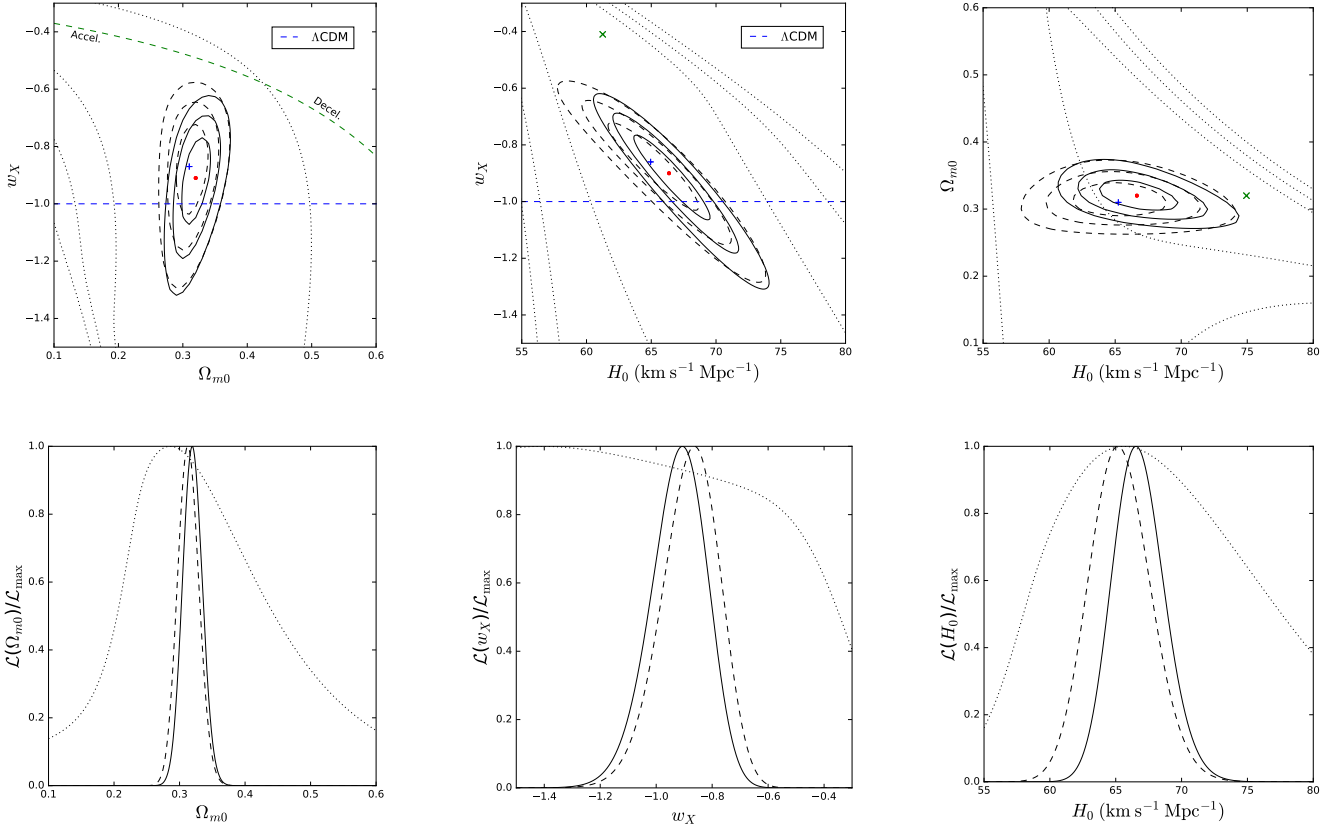


Figure A9. Flat XCDM parametrization with QSO, $H(z)$, and BAO data. Top panels: 1, 2, and 3σ confidence contours and best-fitting points. In the top left and top center panels the horizontal blue dashed line separates quintessence-type parametrizations of dark energy (for which $w_X > -1$) from phantom-type parametrizations of dark energy (for which $w_X < -1$). Points on the blue line (for which $w_X = -1$) correspond to the flat Λ CDM model. The green dashed curve in the left panel separates models that undergo accelerated expansion now from models that undergo decelerated expansion now. Bottom panels: one-dimensional likelihoods for Ω_{m0} , w_X , and H_0 . See text for description and discussion.

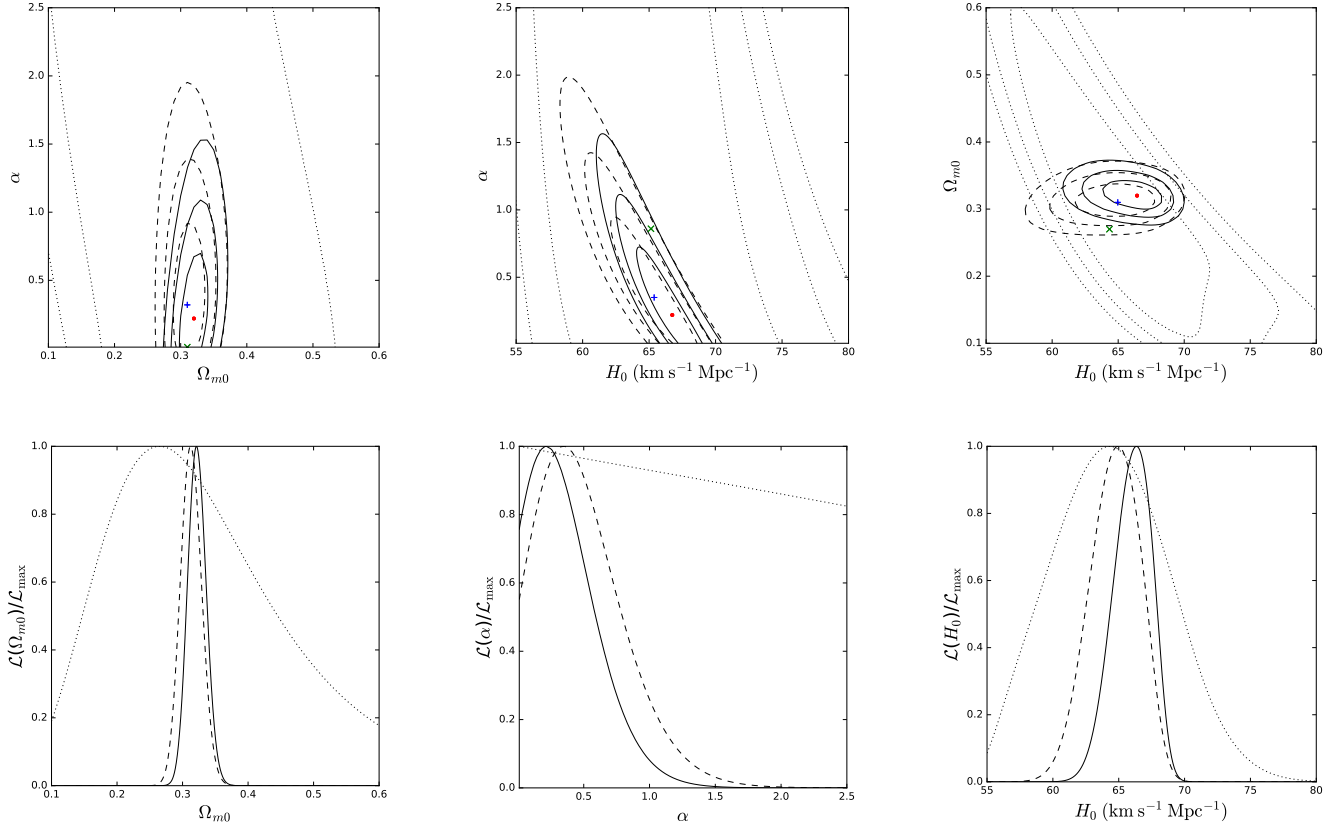


Figure A10. Flat ϕ CDM model with QSO, $H(z)$, and BAO data. Top panels: 1, 2, and 3 σ confidence contours and best-fitting points. Points on the $\alpha = 0$ line in the top left and top center panels correspond to the flat Λ CDM model. Bottom panels: one-dimensional likelihoods of Ω_{m0} , α , and H_0 . See text for description and discussion.

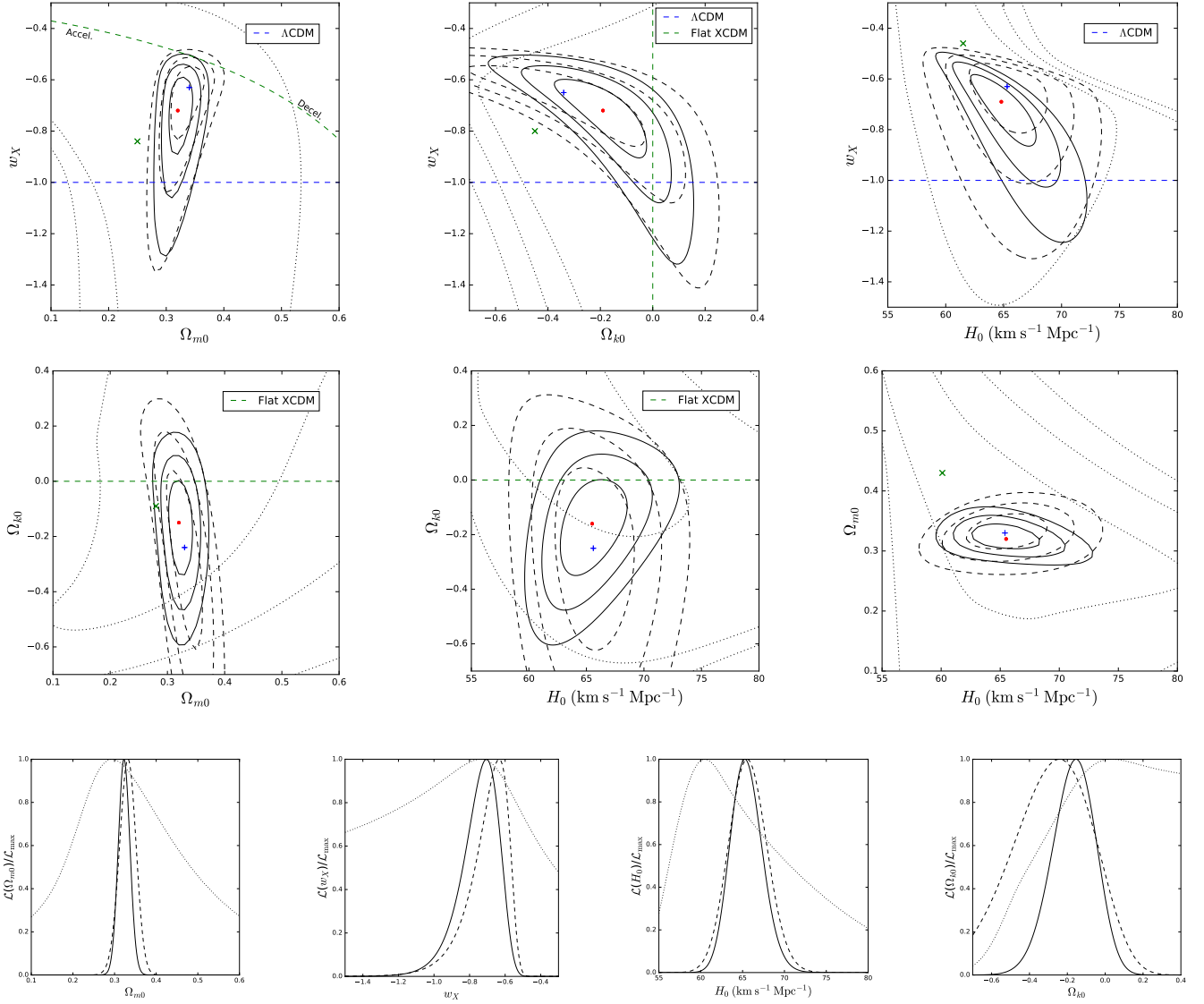


Figure A11. Non-flat XCDM parametrization with QSO, $H(z)$ and BAO data. Top and middle row: 1, 2, and 3σ confidence contours and best-fitting points. In the top panels, the horizontal blue dashed line separates quintessence-type parametrizations of dark energy (for which $w_X > -1$) from phantom-type parametrization of dark energy (for which $w_X < -1$). Points on the blue line (for which $w_X = -1$) correspond to the non-flat Λ CDM model. The green dashed curve in the top left panel separates models that undergo accelerated expansion now from models that undergo decelerated expansion now. The vertical green dashed line in the top center panel, and the horizontal green dashed lines in the left and center panels of the middle row, separate spatially closed models (for which $\Omega_{k0} < 0$) from spatially open models (for which $\Omega_{k0} > 0$). Bottom panels: one-dimensional likelihoods for Ω_{m0} , w_X , H_0 , and Ω_{k0} . See text for description and discussion.

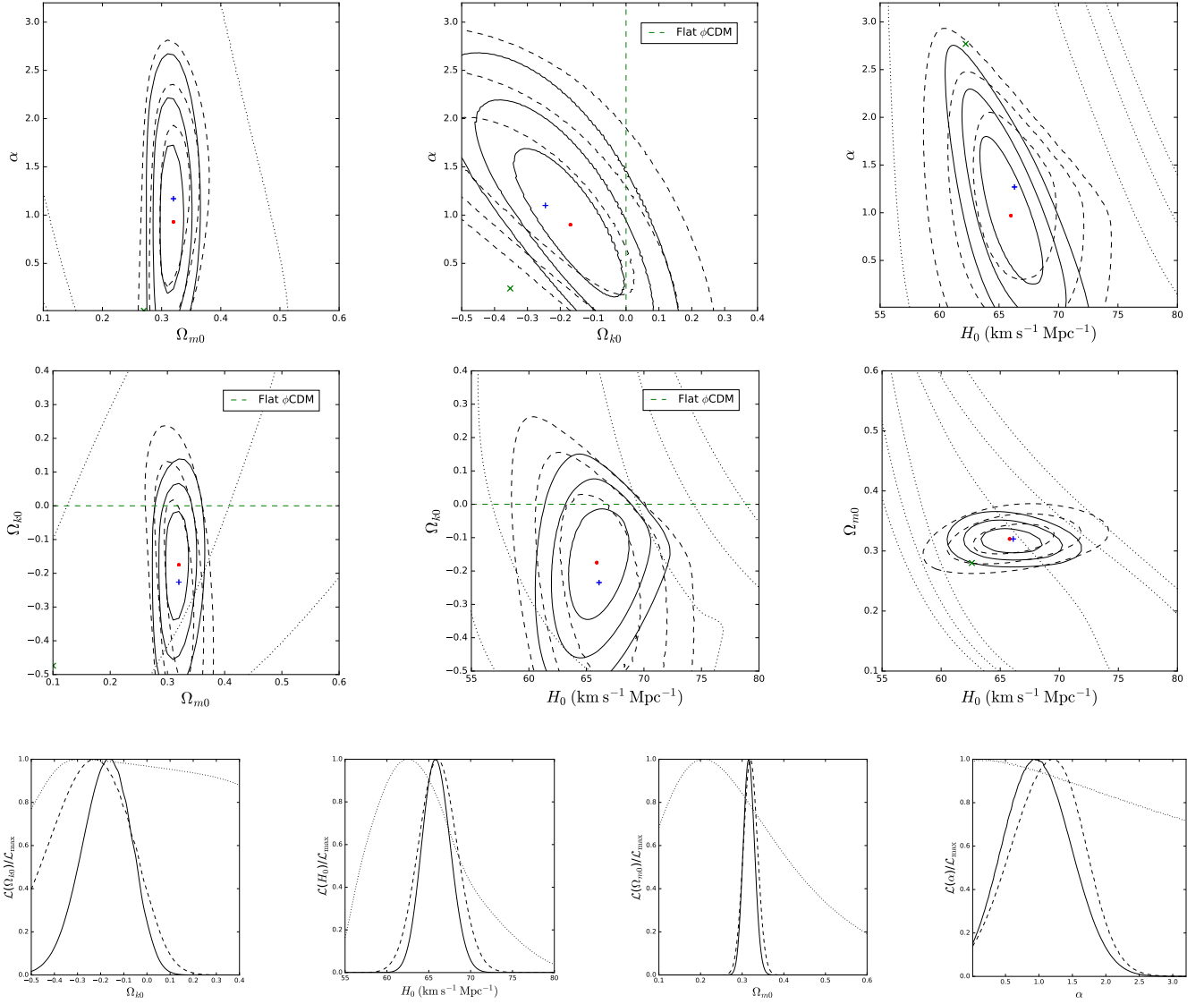


Figure A12. Non-flat ϕ CDM model with $H(z)$ and BAO data. Top and middle rows: 1, 2, and 3 σ confidence contours and best-fitting points. The vertical green dashed line in the top center panel, and the horizontal green dashed lines in the middle left and middle center panels, separate spatially closed models (with $\Omega_{k0} < 0$) from spatially open models (with $\Omega_{k0} > 0$). Points on the $\alpha = 0$ line in the top panels correspond to the non-flat Λ CDM model. Bottom row: one-dimensional likelihoods for Ω_{m0} , α , Ω_{k0} , and H_0 . See text for description and discussion.